

HIGH-RESOLUTION EMISSION-LINE IMAGING OF SEYFERT GALAXIES. I. OBSERVATIONS

CHRISTOPHER A. HANIFF

Institute of Astronomy, Cambridge

ANDREW S. WILSON

Astronomy Program, University of Maryland

AND

MARTIN J. WARD

Department of Astronomy, University of Washington

Received 1988 January 25; accepted 1988 April 27

ABSTRACT

We report a direct imaging survey, conducted with CCD detectors, of 11 Seyfert galaxies (eight type 2's, three type 1's) in [O III] $\lambda\lambda 4959, 5007$, H α + [N II] $\lambda\lambda 6548, 6584$, and their adjacent continua. A mean seeing of 1.3 (FWHM) has enabled the narrow-line regions of all the galaxies to be spatially resolved. Ten of these galaxies contain "linear" radio continuum sources (i.e., double, triple or jetlike straddling the optical continuum nucleus) on the hundreds of parsecs scale, and their VLA maps have been smoothed to the optical seeing to permit a reliable intercomparison. In all 10 galaxies, the [O III] and radio major axes are aligned to within the errors (typically $\leq 5^\circ$). In addition, there is good agreement between the radio and H α axes, and the spatial scales of radio and line-emitting gases are very similar. In some cases, the [O III] image shows double structure associated with the outer radio components. The nature of this close connection between relativistic and thermal gases is assessed in the companion paper.

Subject headings: galaxies: jets — galaxies: Seyfert — galaxies: structure — radio sources: galaxies

I. INTRODUCTION

The narrow-line region (NLR) of active galactic nuclei has received increasing attention during the 1980s. The observed emission-line ratios (e.g., Koski 1978) can be well explained by photoionization models in which a small, central, continuum source illuminates gas clouds with densities ranging between 10^2 and 10^7 cm $^{-3}$ spread over tens to thousands of parsecs (e.g., Ferland and Shields 1985; Ferland and Osterbrock 1986). The continuum source is usually taken to be either nonthermal (power-law spectrum), or thermal emission from an accretion disk, or a composite of thermal sources, the net spectrum of which mimics a power law (see Terlevich and Melnick 1985). Several moderate dispersion studies of the profiles of [O III] $\lambda 5007$ (a strong and relatively uncontaminated line) in the nuclei of active galaxies have been published (e.g., Heckman *et al.* 1981; Véron 1981; Miley and Heckman 1982; Feldman *et al.* 1982; Phillips, Charles, and Baldwin 1983; Heckman, Miley, and Green 1984; Whittle 1985*a, b*; Vrtilek and Carleton 1985). These studies have revealed (see, e.g., the review by Wilson and Heckman 1985) a preferential blueward-slanting asymmetry to the line profiles, a probable blueshift of the mean recession velocity with respect to systemic, a significant correlation between broad and narrow line widths, and correlations between [O III] $\lambda 5007$ width, [O III] $\lambda 5007$ luminosity, and radio luminosity. Models involving radial flow plus dust obscuration (e.g., Heckman *et al.* 1981) or radial flow plus light travel time effects (Capriotti and Foltz 1982) are then implied for the NLR. Other investigators have performed detailed studies of the profiles of a number of different forbidden lines in a relatively small number of objects (e.g., Osterbrock 1981; Penston *et al.* 1984; De Robertis and Osterbrock 1984; Filippenko and Halpern 1984; Filippenko 1985). These papers have demonstrated correlations between line width and either ionization potential or critical density for collisional de-

excitation, emphasizing the large range of densities and velocities present in the NLR. A number of theoretical studies have also been made, some envisaging clouds falling under gravity into the nucleus through a hot medium (e.g., Kwan and Carroll 1982; Carroll and Kwan 1983; Contini and Aldrovandi 1983; Smith 1984), while others (e.g., Krolik and Vrtilek 1984) have analyzed outflow models, in which the line-emitting clouds are entrained in a hot wind.

A continuing problem in all of this work is our ignorance concerning the geometric form of the NLR. Most workers have, for simplicity, assumed spherical symmetry for both the ionizing flux and the gas distribution. However, the presence of "linear" (i.e., double, triple, or "jetlike," straddling the optical nucleus) radio sources in the NLR (e.g., Ulvestad and Wilson 1984*a*) and the correlation between the radio axes and the direction of optical polarization (e.g., Antonucci 1983) indicate the existence of a "preferred axis" in many Seyferts. Since the outer parts of the NLR can be resolved by ground-based telescopes under conditions of good seeing, we have begun a program of direct imaging of the high-excitation circumnuclear gas in Seyfert galaxies. In this paper we present images of the [O III] $\lambda\lambda 4959, 5007$ and H α + [N II] $\lambda\lambda 6548, 6584$ emission lines, and of their adjacent continua, for 11 Seyfert galaxies, 10 of which have "linear" radio structures. The spatial resolution of the images is typically 1"–1.5 (FWHM). By smoothing the VLA¹ radio maps of these galaxies to the optical seeing in our images, we are able to make a precise comparison between the distributions of radio synchrotron and emission-line gas.

In § II we describe the observations and their reduction, while § III presents the results for each individual object. We

¹ The VLA is a facility of the National Radio Astronomy Observatory, which is operated by Associated Universities, Inc., under contract with the National Science Foundation.

demonstrate that the position angles of the [O III], H α , and radio continuum distributions are essentially the same in the 10 objects with "linear" radio structure, and that the spatial scales of relativistic and high-velocity thermal gas are very similar. The nature of this relationship is discussed in depth in the companion paper (Wilson, Ward, and Haniff 1988). In both papers, a Hubble constant of $75 \text{ km s}^{-1} \text{ Mpc}^{-1}$ is assumed.

II. OBSERVATIONS AND REDUCTIONS

All the images presented in this paper were obtained at the $f/10$ Cassegrain focus of the University of Hawaii's 88" telescope on Mauna Kea. Data were collected during four observing runs dated 1985, May 1–May 3, 1986 April 29–May 2, 1986 September 22–September 25, and 1987 February 19–February 22. For the first and last runs, the Institute for Astronomy/Galileo 500 \times 500 pixel CCD was used giving an image scale of $0''.14$ per pixel, while for the remaining two runs the Cambridge GEC 576 \times 385 pixel CCD, which has an effective pixel size of $0''.20$, was employed. Observations of each galaxy were made through narrow-band interference filters centered as close as possible to the redshifted [O III] 4959/5007 lines (on-band) and on the adjacent continuum (off-band). For all galaxies except one (NGC 4051), similar exposures were also taken to isolate the redshifted H α + [N II] lines and their continuum. The weak emission lines [N I] λ 5199 and [O I] λ 6300, 6363 were often included in the off-band filters. However, judging by published line strengths (e.g., Koski 1978), these lines are, in general, sufficiently weak as to make a negligible contribution in comparison with the continuum light. Flat fields were obtained for all of the filters used. Typical FWHM of the filters were 100 Å for the oxygen filters and 150 Å for the hydrogen filters. In order to facilitate subsequent analysis, each galaxy was positioned on the CCD in such a way as to include as many field stars as possible.

The reduction of the data was performed on the Cambridge node of the UK STARLINK computer network. All the frames were corrected for dark current, bias subtracted, and divided by the appropriate flat field. In addition any cosmic-ray events and bad columns were removed interactively. In most cases, we have combined a number of individual on-band and off-band images to improve the signal-to-noise ratio. The emission-line maps were obtained by subtraction of the off-band from the on-band images. Prior to this subtraction it was usually necessary to align, scale, and smooth the separate images. Accurate alignment was achieved by using the field stars as fiducial references. In all cases a shift of origin and perhaps a small rotation ($< 1^\circ$) were sufficient to ensure that the rms position differences between the reference stars in the on-band and off-band images were less than 0.1 pixels. Where fewer than two stars were present, the galaxy core was used as a fiducial reference if it was sufficiently compact in both images. Smoothing of either the on-band or off-band frame was then performed to ensure that the point-spread function was the same in the separate images. Finally, in order to remove the effect of the differences in filter and detector efficiencies at the on-band and off-band peak wavelengths, the continuum frame was multiplied by a scale factor so that the reference stars were removed as completely as possible in the difference map. Unfortunately, in certain cases it was apparent that the field stars had widely different colors, so that an "average" scale factor had to be used. These effects, and the possible differences in color between the reference stars and the galaxies themselves, represent the chief limitation to the detection of faint emission by this technique. We

estimate that our scale factors are accurate to $\sim 5\%$; thus, while the lowest contour present in the difference maps is, to some extent, uncertain, we are confident that the brighter emission has been faithfully reproduced. To facilitate their interpretation, some of the on, off, and difference maps have been smoothed for display. Details of this, together with other relevant observing parameters, are given in Table 1. The absence of suitable reference stars precluded subtraction of off-band from on-band images for Mrk 270, NGC 5135, and the H α image of Mrk 78.

The precise orientation and pixel size of the CCD during each observing run were obtained from frames containing two or more widely separated stars. The separation and position angle of these stars were measured on the Palomar Sky Survey, the local directions of right ascension and declination being deduced from the Ohio State transparent overlays. We estimate that this method is accurate to approximately $\pm 1\%$ for the scale and approximately $\pm 1^\circ$ for the orientation.

III. RESULTS

In this section, we describe the results of the imaging observations for each individual object and compare them with the VLA radio continuum maps. In making such comparisons, it is important to allow for the different spatial resolutions of the optical and radio observations, so, whenever possible, we have convolved the radio maps to the optical seeing. Figures 1–7 and 9–12 present contour maps of the [O III] λ 4959, 5007, H α , adjacent continua, and full resolution, and convolved radio continuum maps for the 11 individual galaxies. These diagrams include the angular and linear scales (the bars in the bottom right-hand corner), the half-power beamwidth when known (the shaded ellipse in the bottom left-hand corner) and the peak of optical continuum light (the cross). Table 2 summarizes and compares the position angles of the isophotal major axes in the circumnuclear region of the various components (emission-line gas, stellar continuum, and radio synchrotron). The position angles listed in columns (2)–(6) of Table 2 are the average major axes of the isophotes over the given angular diameters.

a) Markarian 3 (Seyfert Type 2, Fig. 1)

The [O III] map (Fig. 1a) shows an elongated structure, with the major axis of the brighter isophotes lying in P.A. = $82^\circ \pm 5^\circ$ on the $1''$ – $3''$ scale (Table 2). The isophotes twist toward larger position angles with increasing distance from the peak. The core of the H α image (Fig. 1c) has an identical major axis direction to that of the [O III] core. As can be seen, there is no significant displacement of line and continuum peaks. Faint line emission, best seen in H α , extends almost $5''$ from the nucleus towards the SE and NW. The outer continuum isophotes have major axis P.A. $\approx 17^\circ$ – 22° , unrelated to the circumnuclear line emission. Further in, the continuum isophotes twist, with axis P.A. $\approx 78^\circ \pm 10^\circ$ within $2''$ of the nucleus. This direction is quite similar to the line emission on the same scale. There may, however, be some distortion of the red continuum isophotes through contamination by [O I] λ 6300, 6363, which are relatively strong lines in this galaxy (Koski 1978). Using a spectrum of the nucleus of Mrk 3 covering the region 5950–6880 Å with 3 Å resolution (B. Nath and A. S. Wilson, in preparation), we estimate that [O I] λ 6300, 6363 may contribute up to $\sim 30\%$ of the flux in the nuclear region of our red "continuum" image. Since the spatial dis-

TABLE 1
OBSERVING LOG^a

NAME	DATE	NUMBER OF STARS	CCD	SEEING FWHM	EXPOSURE TIME (s)	BAND	FILTER WAVELENGTHS (Å)			DIFFERENCE MAP: SMOOTHED?
							-50%	Peak	+50%	
Mrk 3	1986 Sep 24	2	CAM	1".1	2 × 150	On	5080	5120	5170	No
	1986 Sep 25	1	CAM	1.4	2 × 150 1 × 100	Off On	5220 6580	5260 6650	5330 6700	
Mrk 6	1987 Feb 19	3	GAL	2.0	2 × 300	On	5080	5120	5170	No
	1987 Feb 19	4	GAL	1.3	2 × 300 2 × 300	Off On	5220 6620	5260 6690	5330 6770	
Mrk 34	1987 Feb 19	1	GAL	1.5	2 × 300	On	5220	5260	5330	Yes
	1987 Feb 19	1	GAL	1.2	2 × 300 2 × 300	Off On	5440 6820	5490 6910	5550 7000	
Mrk 78	1986 Apr 30	2	CAM	1.4	1 × 300	On	5150	5200	5250	Yes
	1986 Apr 30	2	CAM	1.3	2 × 120 2 × 120	On Off	6700 6620	6770 6690	6840 6770	
Mrk 79	1986 May 1	0	CAM	1-2?	2 × 300	On	5080	5120	5170	No
	1986 May 1	0	CAM	1-2?	2 × 300 1 × 300	Off On	5150 6620	5200 6700	5250 6770	
Mrk 270	1987 Feb 19	0	GAL	1-2?	2 × 300	On	4950	5000	5040	N/A
	1987 Feb 19	0	GAL	1-2?	2 × 300 2 × 300	Off On	5100 6580	5150 6650	5190 6700	
Mrk 573	1986 Sep 23	2	CAM	1.6	2 × 600	On	5080	5120	5170	No
	1986 Sep 25	2	CAM	1.1	2 × 600 2 × 300	Off On	5220 6620	5260 6690	5330 6770	
Mrk 1066	1986 Sep 24	1	CAM	1.2	2 × 600	On	5080	5120	5170	No
	1986 Sep 25	5	CAM	1.0	2 × 500 1 × 500	On Off	6580 6380	6650 6430	6700 6470	
NGC 591	1986 Sep 24	3	CAM	1.2	2 × 600	On	5080	5120	5170	No
	1986 Sep 25	3	CAM	1.0	2 × 600 1 × 500	Off On	5220 6580	5260 6650	5330 6700	
NGC 4051	1985 May 2	0	GAL	1.1	2 × 300	On	4950	5000	5040	Yes
					2 × 300	Off	5080	5120	5170	
NGC 5135	1987 Feb 20	0	GAL	1-2?	2 × 300	On	5080	5120	5170	N/A
	1987 Feb 20	0	GAL	1-2?	2 × 300 2 × 300	Off On	5150 6580	5200 6650	5250 6700	
					2 × 300	Off	6380	6430	6470	N/A

^a The columns of this table give (from left to right): name of the galaxy, date of observation, number of stars used in aligning the on- and off-band frames, the CCD used (GAL = IfA Galileo, CAM = Cambridge GEC), the seeing, exposure time, the filter wavelengths (at peak and at 50% of peak transmission) and an indication of whether the difference map was smoothed by binning together 3 × 3 pixels, but retaining sampling at the original pixel locations.

TABLE 2
POSITION ANGLES OF ISOPHOTAL MAJOR AXES^a

Name (1)	Radio (2)	[O III] (3)	H α (4)	Continuum near [O III] (5)	Continuum near H α (6)	Radio Minus [O III] (7)	Radio Minus H α (8)	Radio Minus Continuum Near [O III] (9)	Radio Minus Continuum Near H α (10)
Mrk 3	85°(1".4)	82°(1"-3")	81°(1"-3")	70°(1"-2")	...	+3°	+4°	+15°	...
Mrk 6	178°(1".0)	8°(3")	-10°
Mrk 34	156°(2".4)	148°(3")	150°(3")	130°(6")	118°(8")	+8°	+6°	+26°	+38°
Mrk 78	89°(4")	84°(2"-7")	(83°)(2"-6")	75°(2"-7")	83°(2"-7")	+5°	(+6°)	+14°	+6°
Mrk 79	9°(3")	9°(1"-3")	0°
Mrk 270	50°(2".3)	58°(3")	(61°)(3")	-8°	(-11°)
Mrk 573	122°(2".9)	116°(2"-8")	110°(2"-6")	101°(2"-6")	103°(2"-6")	+3°	+12°	+21°	+19°
Mrk 1066	134°(2".8)	131°(3")	126°(2"-3")	119°(2")	121°(2")	+3°	+8°	+15°	+13°
NGC 4051	78°(0".4-1".5)	81°(2".5)	...	(159°)(6")	...	-3°	...	(-81°)	...
NGC 5135	30°(1"-4")	2°(1"-3")	+28°

^a Cols. (2)-(6) give the position angles (in degrees) of the major axes of the radio and optical images followed, in parentheses, by the spatial scale (in arcsec) to which the position angle refers. Col. (7)-(10) give the differences of position angle (in degrees) between the radio and optical isophotal major axes. Position angles enclosed in parentheses are uncertain (see text).

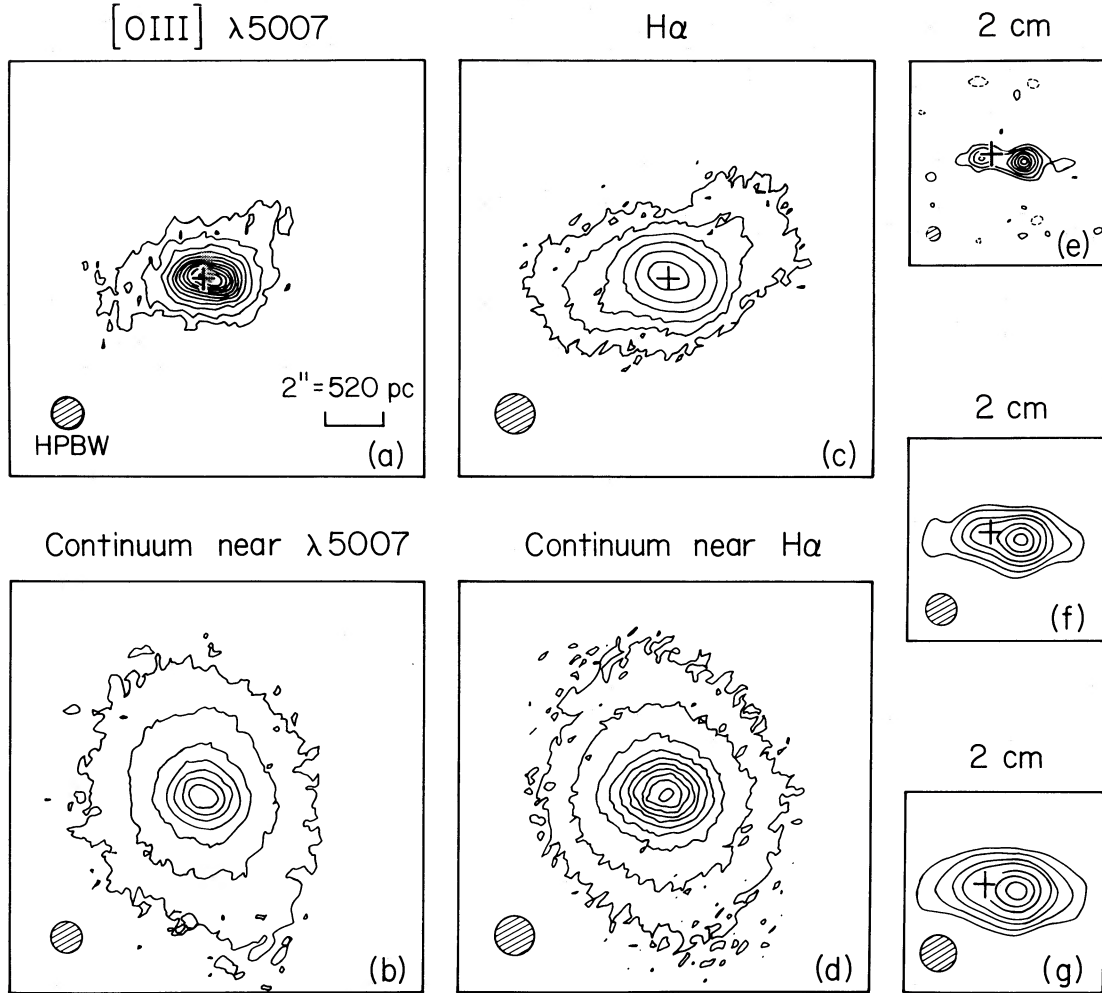


FIG. 1.—Mrk 3. (a) $[\text{O III}] \lambda 5007$, contours at 50, 100, 200, 300, 400, 500, 600, 700, 800, 900, 1000, and 1100. (b) Continuum near $\lambda 5007$, contours at 50, 100, 200, 300, 400, 500, and 600. (c) $\text{H}\alpha$, contours at 100, 200, 400, 800, 1600, and 3200. (d) Continuum near $\text{H}\alpha$, contours at 100, 200, 400, 600, 800, 1000, 1200, 1400, 1600, and 1800. (e) 2 cm VLA map with $0''.5$ resolution, contours at -5% , 5% , 10% , 20% , 30% , 50% , 70% , and 90% of the peak brightness of $45.0 \text{ mJy (beam area)}^{-1}$. (f) As (e), but smoothed to the same resolution ($1''.1$ FWHM) as (a) and (b); contours are plotted at the same percentages as (e), with the peak being $55.1 \text{ mJy (beam area)}^{-1}$. (g) As (e), but smoothed to the same resolution ($1''.4$) as (c) and (d); contours are plotted at the same percentages as (e), with the peak being $59.5 \text{ mJy (beam area)}^{-1}$.

FIG. 1–7 and 9–12.—These diagrams show optical and radio isophotes for the program galaxies, ordered by increasing Markarian number and then by increasing NGC number. North is up, and east to the left. In all cases except one (NGC 4051), the axes of the pixel directions of the CCD coincide with right ascension and declination to within 3° , and no correcting tilt has been applied to the diagrams. For NGC 4051 (Fig. 11), the radio panels are tilted to the same orientation as the optical. In most figures, the spatial scale of each panel is identical and is indicated only in the top left panel (a). When this is not so, the scale is given separately on each panel. The shaded circle or ellipse in the bottom left-hand corner of each panel gives the beam size (seeing FWHM for optical images when known from stars in the field; half-power beam width of clean restoring beam for radio maps). The crosses represent the peak of optical continuum light. For the emission-line images, this location was determined from the adjacent off-band image, after alignment of the reference stars. For the radio maps, the absolute right ascension and declination of the optical nucleus (from Clements 1981, 1983) was used. The on-band minus off-band difference maps, showing the distribution of emission-line gas, are labeled “ $[\text{O III}] \lambda 5007$ ” and “ $\text{H}\alpha$.” The off-band images are labeled “continuum near $\lambda 5007$ ” and “continuum near $\text{H}\alpha$.” When subtraction of off-band from on-band images was not feasible (§ II), the difference maps are replaced by the on-band images (“ $[\text{O III}] \lambda 5007$ On-Band” and “ $\text{H}\alpha$ On-Band”). The right-hand panels are the radio maps (from Ulvestad, Wilson, and Sramek 1981; Ulvestad and Wilson 1984a, b, 1988). When possible, a high-resolution ($\leq 0''.5$) radio map is given along with maps convolved to exactly the same resolution as the optical images. Units of contour levels of the optical images are counts above background.

tribution of these lines is unknown, we cannot correct the continuum isophotes for this contamination.

In radio continuum radiation, Mrk 3 is dominated by two components of separation $1''.4$ (Wilson *et al.* 1980; Pedlar, Unger, and Booler 1984; Ulvestad and Wilson 1984a), as shown in Figure 1e. Radio maps smoothed to the $[\text{O III}]$ and $\text{H}\alpha$ distributions are shown in Figures 1f and 1g, respectively. The optical position measured by Clements (1981) has errors roughly $\pm 0''.2$ – $0''.3$, so the exact location of the optical nucleus in relation to the two radio components is uncertain. The axis

of the radio source is in P.A. = $85^\circ \pm 2^\circ$, consistent with that of the line images. Profiles of the $\lambda 2 \text{ cm}$ and $[\text{O III}]$ distributions along their mutual major axis indicate, however, that the two components which dominate the radio continuum are less prominent in the optical line emission.

b) Markarian 6 (Seyfert Type 1.5, Fig. 2)

The $[\text{O III}]$ image (Fig. 2a) was obtained under poor observing conditions (high winds and $2''.0$ seeing) and reveals little more than a bright, essentially unresolved, source coincident

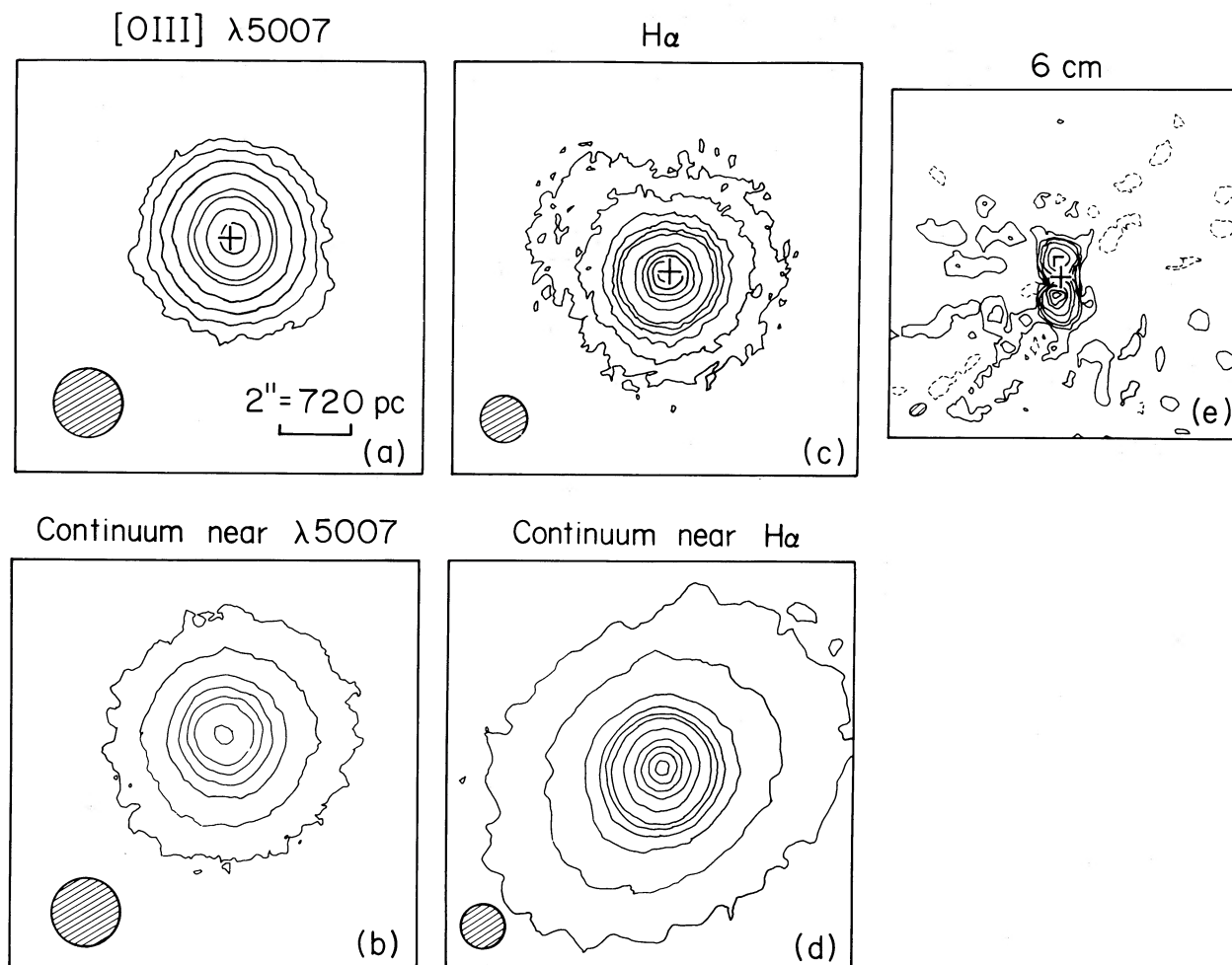


FIG. 2.—Mrk 6. (a) [O III] $\lambda 5007$, contours at 50, 100, 200, 400, 800, 1000, 1500, and 2000. (b) Continuum near $\lambda 5007$, contours at 100, 200, 400, 600, 800, 1000, and 1500. (c) H α , contours at 100, 200, 400, 600, 800, 1000, 2000, 3000, 4000, 5000, and 6000. (d) Continuum near H α , contours at 100, 200, 400, 600, 800, 1000, 2000, 4000, 6000, 8000, and 10,000. (e) 6 cm VLA map with $0''.3 \times 0''.6$ resolution, contours at $-0.5, 0.5, 1, 1.5, 2.4, 4.8, 9.6, 14.4,$ and 19.2 mJy (beam area) $^{-1}$.

with the continuum peak. The inner isophotes appear elliptical with a major axis in P.A. = $8^\circ \pm 5^\circ$, but given the low quality of the data, this result needs to be confirmed with a higher resolution image. The star images in the off-band H α image (Fig. 2d) are, unfortunately, slightly elliptical, which produces a spurious E-W elongation in the bright core of the H α difference map (Fig. 2c). We believe that the fainter isophotes in the red images are reliable.

At radio wavelengths (Fig. 2e), Mrk 6 is a double of separation $1''.0$ in P.A. = $178^\circ \pm 2^\circ$ (Ulvestad, Wilson and Sramek 1981; Ulvestad and Wilson 1984a), close to the direction of the [O III] major axis. Unfortunately, it was not possible to smooth the $\lambda 6$ cm map to the optical seeing because this early VLA map is no longer available in digital format.

c) Markarian 34 (Seyfert Type 2, Fig. 3)

Both the [O III] (Fig. 3a) and H α (Fig. 3c) images are elongated in P.A. = 148° – 150° and are only marginally, if at all, resolved in the perpendicular direction. This morphology is confirmed by independent observations during a separate observing run. Both line images are consistent with a (deconvolved) FWHM $\approx 2''.5 \pm 0''.5$ in the major axis direction.

The H α image, which was obtained under better seeing conditions, strongly suggests that the emission-line morphology may actually be double and straddle the optical continuum nucleus. This interesting result should be confirmed by images in somewhat better seeing ($0''.5$ – $1''.0$). The stars in the off-band [O III] image are slightly elliptical, but an independent exposure taken during the 1985 May run confirms the NW-SE elongation of the continuum isophotes.

The radio maps (Figs. 3e, 3f, and 3g) show a double source straddling the optical nucleus in P.A. = $156^\circ \pm 2^\circ$ and with separation $2''.4$ (Ulvestad and Wilson 1984a). The emission-line and radio continuum morphologies are, therefore, remarkably similar in this galaxy. Interestingly, this similarity includes the relative brightnesses of the SE and NW components (cf. Figs. 3c and 3g). Intercomparison of the emission-line and radio continuum profiles along their mutual major axis suggests that there may be, in addition to the double structure, a more centrally concentrated component to the emission-line region.

d) Markarian 78 (Seyfert Type 2, Fig. 4)

Comparison of the [O III] (Fig. 4a) and adjacent continuum images (Fig. 4b) shows that the line and continuum peaks are

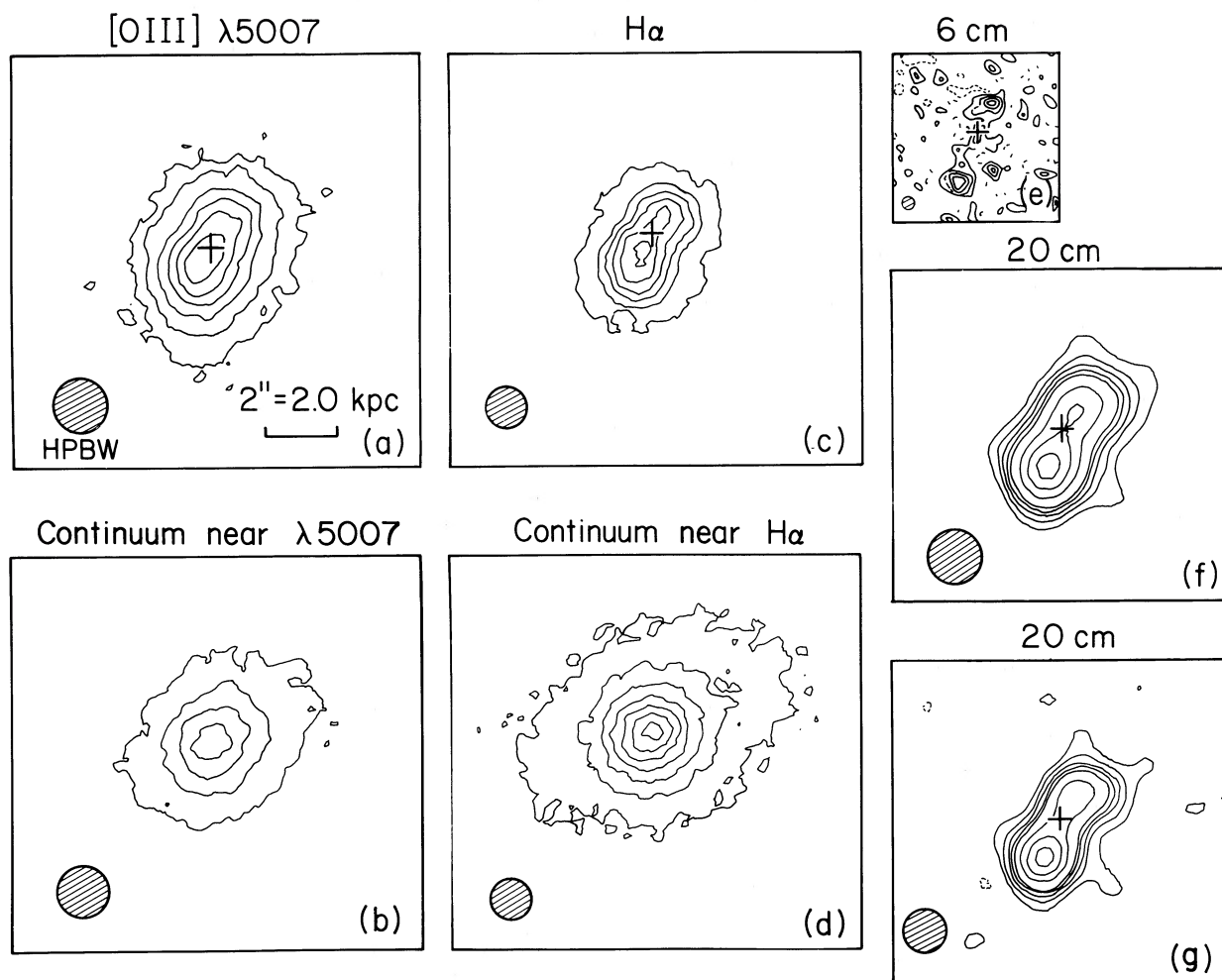


FIG. 3.—Mrk 34. (a) [O III] $\lambda 5007$, contours at 50, 100, 200, 300, 400, and 500. (b) Continuum near $\lambda 5007$, contours at 100, 200, 300, and 400. (c) $H\alpha$, contours at 50, 200, 300, 400, 500, and 600. (d) Continuum near $H\alpha$, contours at 100, 200, 300, 400, 500, 600, and 700. (e) 6 cm VLA map with $0''.34 \times 0''.34$ resolution, contours at -20% , 20% , 40% , 60% , and 80% of the peak brightness of $1.52 \text{ mJy (beam area)}^{-1}$. (f) 20 cm VLA map with the same resolution ($1''.5$) and scale as (a) and (b); contours are plotted at -6% , 6% , 12% , 18% , 24% , 30% , 50% , 70% , and 90% of the peak brightness of $8.7 \text{ mJy (beam area)}^{-1}$. (g) As (f), but with the same resolution ($1''.2$) and scale as (c) and (d); contours are plotted at the same percentages as in (f), with the peak being $7.8 \text{ mJy (beam area)}^{-1}$.

not coincident. The brightest [O III] emission lies $\sim 1''$ east of the continuum peak. The overall [O III] image is indicative of a double-lobed structure with separation $2''.6$ in P.A. $= 84^\circ \pm 3^\circ$, in agreement with the findings of Adams (1973). These two optical clouds are known to be kinematically distinct, with a difference in velocity of $\sim 1000 \text{ km s}^{-1}$ (Boksenberg 1977; Vrtilek and Carleton 1985; De Robertis 1987). The peak to the west of the nucleus is dominated by the blueshifted component (component C of Whittle *et al.* 1988). This peak is somewhat reduced in intensity in our [O III] image (Fig. 4a), because its wavelength corresponds to a lower filter transmission than does the wavelength of the redshifted component to the east of the nucleus. Unfortunately, we have been unable to produce an $H\alpha$ difference map due to lack of suitable reference stars. The on-band $H\alpha$ image (Fig. 4c) is, nevertheless, qualitatively consistent with the [O III] picture.

The VLA maps (Figs. 4e, 4f, from Ulvestad, Wilson, and Sramek 1981) reveal a triple source plus fainter extended emission, with the central component of the triple coincident with

Clements's (1981) position of the optical continuum nucleus. The major axis of the radio triple lies in P.A. $= 89^\circ \pm 3^\circ$, essentially the same as the [O III] emission. The separation of the outer radio lobes in Figure 3e is $3''.3$. For the same reason that applied to Mrk 6, it has not been possible to smooth the radio map to the optical resolution. Part of the small difference ($2''.6$ vs. $3''.3$) between the radio and optical cloud separations probably results from the difference in beam size. The presence of faint extended emission between the central and outer radio components has the effect of reducing the apparent radio component separation at lower resolutions.² Thus, the data indicate that the two [O III] clouds are largely associated with the radio components. The major axis of the optical continuum light lies in P.A. $\approx 75^\circ$ – 83° which is close to, but probably significantly different from, the radio axis.

² This effect may contribute to the apparent difference in the separations of the double radio and double [O III] $\lambda 5007$ components in NGC 5929 found by Whittle *et al.* (1986).

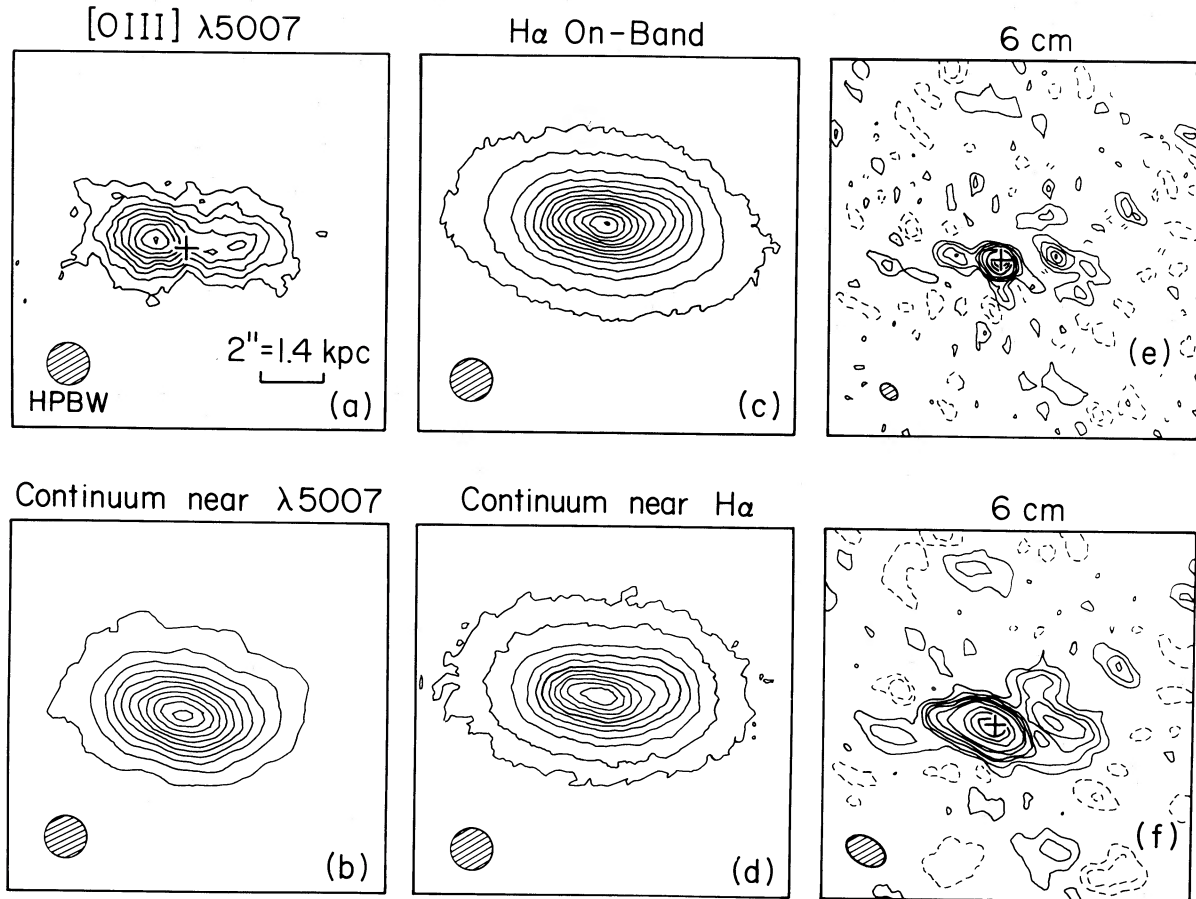


FIG. 4.—Mrk 78. (a) $[\text{O III}] \lambda 5007$ contours at 10, 20, 30, 40, 50, 60, 70, 80, and 90. (b) Continuum near $\lambda 5007$, contours at 10, 20, 30, 40, 50, 60, 70, 80, 90, 100, and 110. (c) $\text{H}\alpha$ on-band (not continuum subtracted), contours at 125, 250, 500, 750, 1000, 1250, 1500, 1750, 2000, 2250, 2500, 2750, 3000, and 3250. (d) Continuum near $\text{H}\alpha$, contours at 50, 100, 200, 300, 400, 500, 600, 700, 800, 900, and 1000. (e) 6 cm VLA map with resolution $0''.5 \times 0''.7$, contours at $-0.36, -0.18, 0.18, 0.36, 0.6, 0.9, 1.2, 2.4, 3.6,$ and $4.8 \text{ mJy (beam area)}^{-1}$. (f) 6 cm VLA map with resolution $0''.8 \times 1''.4$, contours at $-0.35, -0.18, 0.18, 0.35, 0.53, 0.7, 1.05, 1.4, 2.8, 4.2,$ and $5.6 \text{ mJy (beam area)}^{-1}$.

e) Markarian 79 (Seyfert Type 1.2, Fig. 5)

Because no reference stars were present in the frames of this galaxy, alignment and scaling of on-band and off-band frames were performed using the nucleus of the galaxy and an H II region. The $[\text{O III}]$ map (Fig. 5a) shows a very compact source which is resolved along its major axis, P.A. = $9^\circ \pm 5^\circ$. If we assume the $[\text{O III}]$ emission is unresolved along its minor axis, the seeing is $\sim 1''.5$. A very uncertain deconvolution from this seeing along the major axis dimension suggests an intrinsic FWHM $\approx 1''.0$. For the $\text{H}\alpha$ band data, the slight ellipticity in the core of the continuum (Fig. 5d) is not real but a consequence of trailing. The effect on the difference map (Fig. 5c) is to produce a spurious elongation in the orthogonal direction. Thus, apart from indicating the overall spatial extent of the emission, Figures 5c and 5d provide no useful information on the morphology of the core source.

At radio wavelengths, Mrk 79 is a triple source (Ulvestad and Wilson 1984a) with major axis in P.A. $\approx 9^\circ \pm 3^\circ$, the same as the axis of the $[\text{O III}]$ emission. The overall extent of the triple is $\sim 3''.6$ (Fig. 5f), and the separation of the nuclear component from the southern component $\sim 1''.0$ (Fig. 5e).

f) Markarian 270 (Seyfert Type 2, Fig. 6)

Because of the absence of reference stars in the CCD frames of this galaxy, it was not possible to form on-band minus off-band difference maps. The on-band and off-band images are presented in Figures 6a–6d. The $[\text{O III}]$ on-band and off-band images are clearly different, indicating the presence of an elongated $[\text{O III}]$ emission region extending $\sim 3''$ in P.A. = $58^\circ \pm 5^\circ$. The elongation of the $\text{H}\alpha$ emission is less clear, but appears to be in roughly the same direction.

The radio structure of Mrk 270 is a double of separation $2''.3$ in P.A. = $50^\circ \pm 2^\circ$ (Ulvestad and Wilson 1984a). As for the other objects, then, the radio and $[\text{O III}]$ major axes are very similar. A more detailed comparison is not possible because of the absence of reference stars within our field of view, which precludes not only the production of difference maps but also determination of the optical seeing.

g) Markarian 573 (Seyfert Type 2, Fig. 7)

The $[\text{O III}]$ distribution extends $\sim 9''$ in P.A. $\approx 116^\circ \pm 2^\circ$. The $\text{H}\alpha$ emission has a similar position angle ($110^\circ \pm 3^\circ$) and extent ($\sim 13''$), but is wider than the $[\text{O III}]$ emission in the

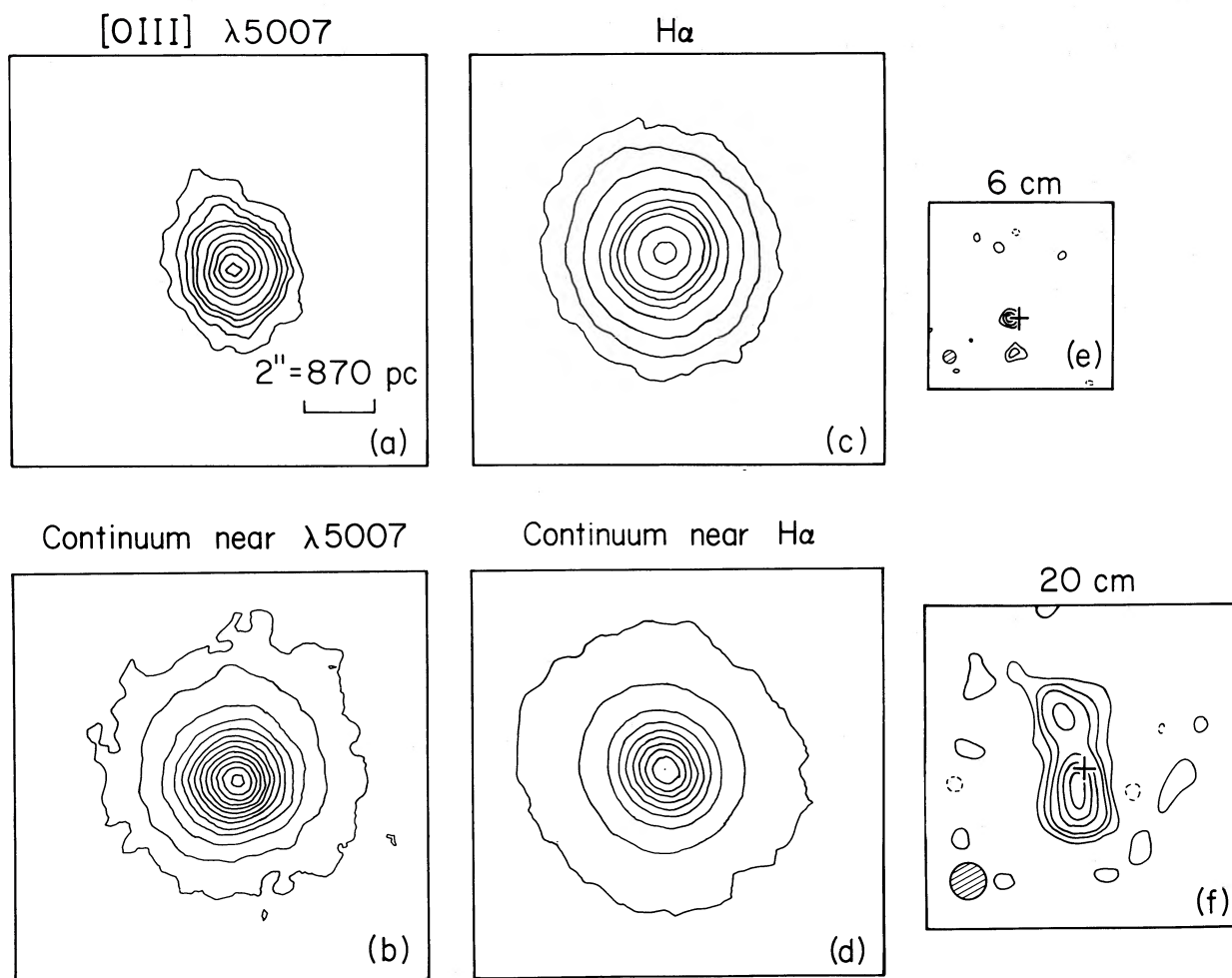


FIG. 5.—Mrk 79 (a) [O III] $\lambda 5007$, contours at 20, 40, 60, 80, 100, 150, 200, 250, 300, and 350. (b) Continuum near $\lambda 5007$, contours at 25, 50, 100, 150, 200, 250, 300, 350, 400, 450, 500, 550, and 600. (c) $H\alpha$, contours at 50, 100, 200, 400, 600, 800, 1000, 1500, and 2000. (d) Continuum near $H\alpha$, contours at 100, 200, 400, 600, 800, 1000, 1200, 1400, 1600, and 1800. (e) 6 cm VLA map with resolution $0''.4 \times 0''.3$, contours at -30% , 30% , 45% , 60% , 75% , and 90% of the peak brightness of $1.3 \text{ mJy (beam area)}^{-1}$. (f) 20 cm VLA map with resolution $1''.2 \times 1''.1$, contours at -10% , 10% , 20% , 30% , 50% , 70% , and 90% of the peak brightness of $3.6 \text{ mJy (beam area)}^{-1}$.

minor axis direction. The continuum isophotes on the same spatial scale as the emission-line gas have a major axis P.A. = $102^\circ \pm 5^\circ$. As for Mrk 3 and Mrk 78, this axis is close to, but significantly different from, the major axis of the line emission. The peaks of line and continuum light distributions are coincident.

The right panels of Figure 7 show three VLA 6 cm maps of Mrk 573 (Ulvestad and Wilson 1984a). The full resolution image (Fig. 7e) reveals a triple source with outer radio components separated by $2''.9$ in P.A. = $124^\circ \pm 3^\circ$. After smoothing to the resolution of the [O III] image (Fig. 7f), this position angle becomes $119^\circ \pm 3^\circ$, which is identical to the [O III] major axis to within the errors. The agreement with the $H\alpha$ image (see Figs. 7c and 7g) is less good, with the radio position angle at $122^\circ \pm 3^\circ$ and the $H\alpha$ position angle at $110^\circ \pm 3^\circ$.

A comparison of the distribution of [O III] and 6 cm radio radiation is afforded by profile plots along their common major axis (Fig. 8). Here we have assumed that the central radio component is coincident with the optical continuum peak; this is consistent with Clements' (1981) astrometric posi-

tion for the nucleus (Fig. 7e). The line and radio distributions are quite different in detail (Fig. 8). The "humps" in the 6 cm profile some $1''$ west and $1''.3$ east of the nucleus correspond to the outer radio lobes smoothed to the lower resolution of the [O III] image. In contrast, the [O III] distribution shows a well-defined central peak and only a hint of a shoulder some $2''$ west of the nucleus. Thus the [O III] emission is more concentrated towards the nucleus than is the radio, and the line emission at the position of the discrete radio lobes themselves is relatively weak.

h) Markarian 1066 (Seyfert Type 2, Fig. 9)

The [O III] image (Fig. 9a) is suggestive of a double structure of separation $0''.8$, with the continuum nucleus in between. Since this separation is somewhat below the FWHM of the seeing ($1''.2$), the reality of this double needs to be confirmed with a higher resolution observation. The [O III] line emission extends over $\sim 3''.3$, with outer isophotes in P.A. = $131^\circ \pm 10^\circ$. The possible double structure seems to have a smaller position angle. The $H\alpha$ emission (Fig. 9c) shows no hint of the double

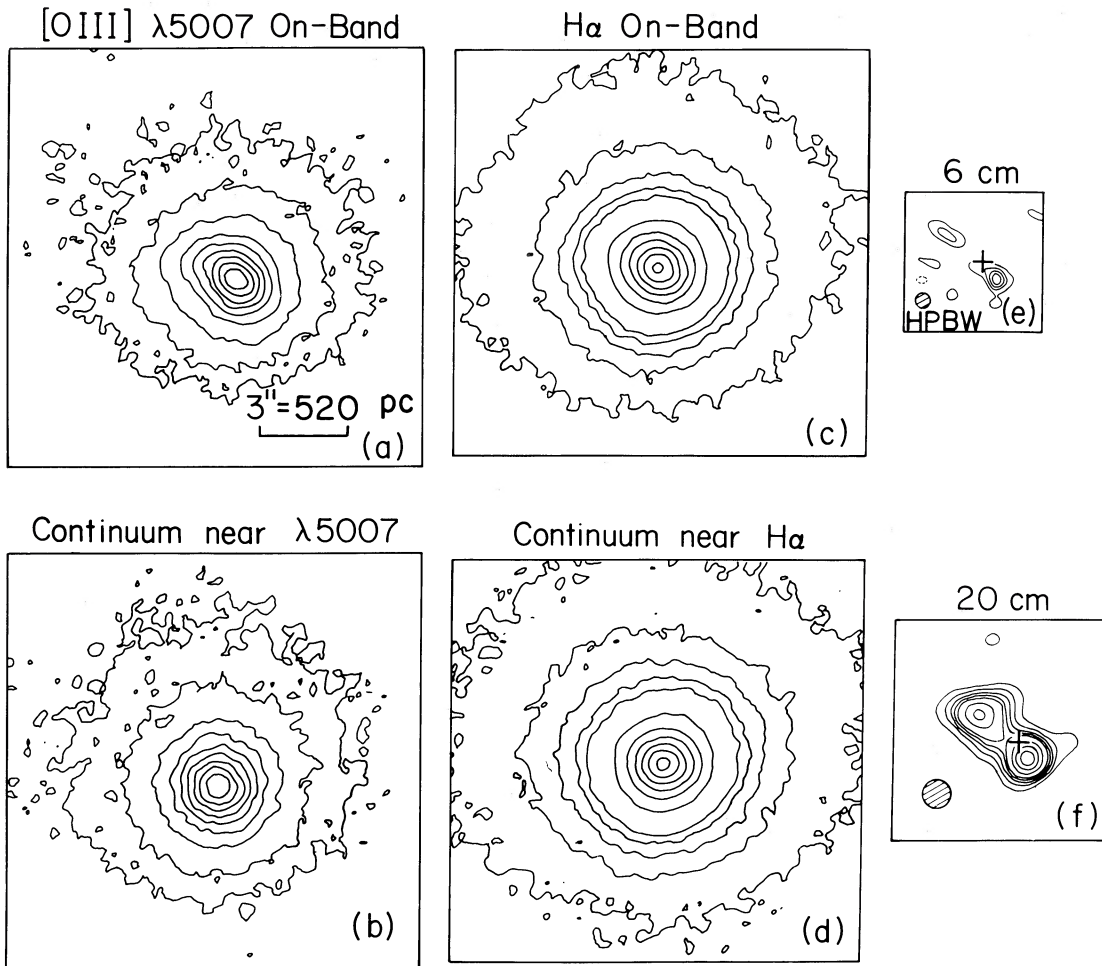


FIG. 6.—Mrk 270. (a) [O III] $\lambda 5007$ on-band (not continuum subtracted), contours at 50, 100, 200, 400, 600, 800, 1000, and 1200. (b) Continuum near $\lambda 5007$, contours at 50, 100, 200, 300, 400, 500, 600, 700, and 800. (c) $H\alpha$ on-band (not continuum subtracted), contours at 100, 200, 300, 400, 500, 1000, 1500, 2000, 2500, 3000, and 3500. (d) Continuum near $H\alpha$, contours at 100, 200, 300, 400, 500, 1000, 1500, 2000, 2500, 3000, and 3500. (e) 6 cm VLA map with $0''.5$ resolution, contours at -20% , 20% , 30% , 50% , 70% , and 90% of the peak brightness of $1.77 \text{ mJy (beam area)}^{-1}$. (f) 20 cm VLA map with $1''.0$ resolution, contours at -6% , 6% , 12% , 18% , 24% , 30% , 50% , 70% , and 90% of the peak brightness of $5.28 \text{ mJy (beam area)}^{-1}$.

structure, and its peak coincides accurately with the continuum peak. The elongation (P.A. $\approx 126^\circ$) of the brighter isophotes of the $H\alpha$ image is quite similar to that of the [O III] picture. The bright circumnuclear continuum light (Figs. 9b, 9d) has P.A. $\approx 120^\circ \pm 3^\circ$.

At radio wavelengths, Mrk 1066 is a “linear,” probably triple, source extending $2''.8$ in P.A. = $134^\circ \pm 4^\circ$ (see Figs. 9e, 9f, and 9g, from Ulvestad and Wilson 1988), in excellent agreement with the line and, to a lesser extent, with the continuum major axes. The overall extents of the radio and [O III] emissions are similar.

i) NGC 591 = Markarian 1157 (Seyfert type 2, Fig. 10)

This galaxy shows a more compact line-emitting region than the other objects. The [O III] image (Fig. 10a) is marginally resolved in the NW–SE direction. In the light of $H\alpha$ (Fig. 10c), low-excitation gas may extend as far as $16''$ to east and west of the nucleus; note, however, that the lowest contour in this image may not be reliable. The nuclear line and continuum peaks are coincident.

A recent VLA map (Ulvestad and Wilson 1988) is shown in Figure 10e. The radio source is a double, with separation $0''.6$ in P.A. = $152^\circ \pm 4^\circ$. After smoothing to the resolution of the optical images (Figs. 10f and 10g), only a general NW–SE elongation, similar to the [O III] image, may be discerned. Higher resolution optical measurements are needed to define in detail the relationship between emission-line and radio continuum radiation in this object.

j) NGC 4051 (Seyfert Type 1, Fig. 11)

This is the only case in which an on-band minus off-band difference map was formed when no reference stars were present. The very compact galaxy core was used to align the images and the outer parts of the galaxy were used to obtain the scaling factor. The seeing given in Table 1 represents the FWHM along the minor axis of the [O III] image.

The [O III] image (Fig. 11a) shows a very compact emission-line region of overall extent $\leq 3''$ in P.A. $\approx 81^\circ \pm 5^\circ$. A very uncertain Gaussian deconvolution from the seeing suggests an intrinsic FWHM $\approx 0''.5\text{--}0''.8$ along this axis. Radio maps (from

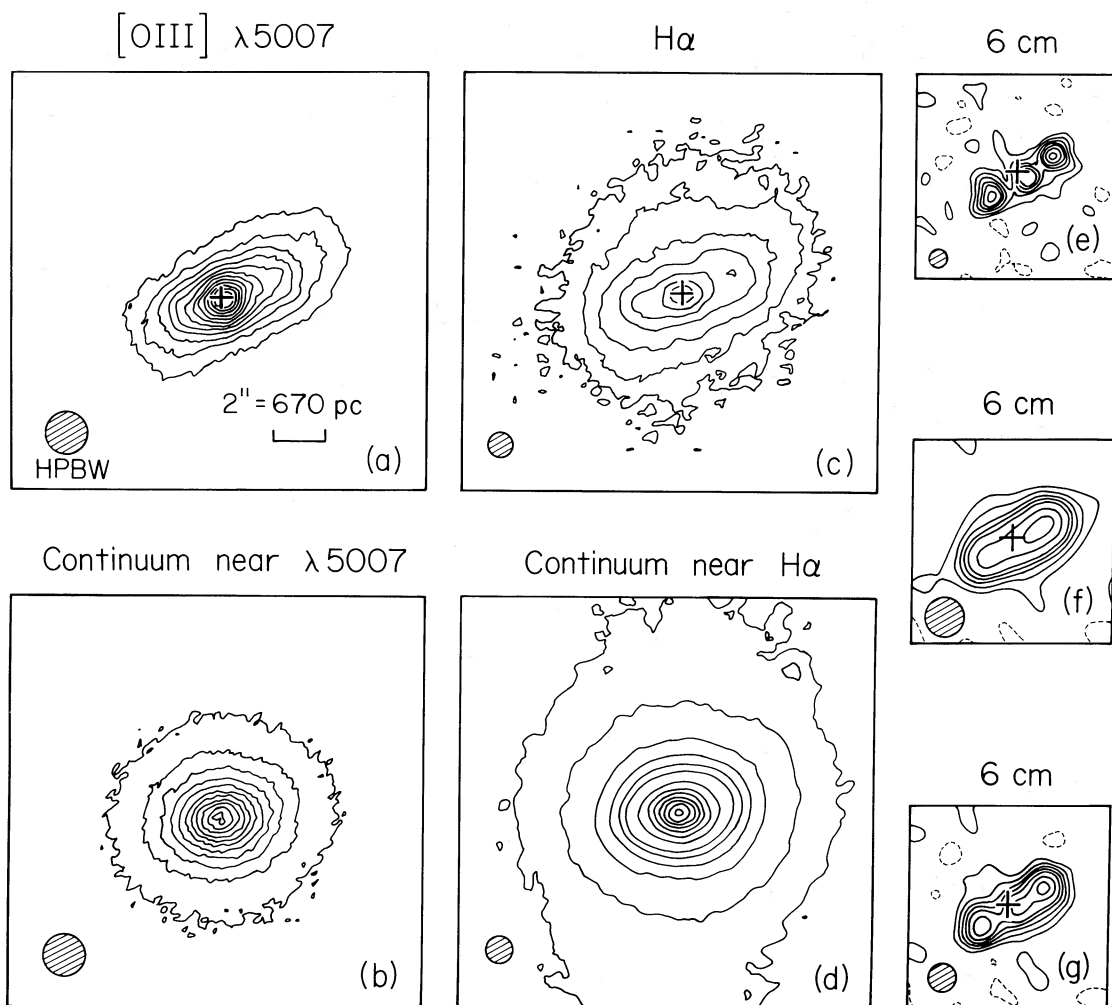


FIG. 7.—Mrk 573. (a) $[\text{O III}] \lambda 5007$, contours at 100, 200, 300, 400, 500, 600, 700, 800, 900, 1000, 1100, 1200, and 1300. (b) Continuum near $\lambda 5007$ contours at 50, 100, 200, 300, 400, 500, 600, 700, 800, 900, and 1000. (c) $\text{H}\alpha$, contours at 75, 150, 300, 600, 1000, 1500, and 2000. (d) Continuum near $\text{H}\alpha$, contours at 100, 200, 400, 600, 800, 1000, 1500, 2000, 2500, 3000, 3500, 4000, and 4500. (e) 6 cm VLAMAP with $0.7''$ resolution, contours at -10% , 10% , 20% , 30% , 40% , 50% , 70% , and 90% of the peak brightness of $1.4 \text{ mJy (beam area)}^{-1}$. (f) As (e), but smoothed to the same resolution ($1.6''$) as panels (a) and (b); contours are plotted at the same percentages as in (e), with the peak being $2.1 \text{ mJy (beam area)}^{-1}$. (g) As (e), but smoothed to the same resolution ($1.1''$) as (c) and (d); contours are plotted at the same percentages as in (e), with the peak being $1.6 \text{ mJy (beam area)}^{-1}$.

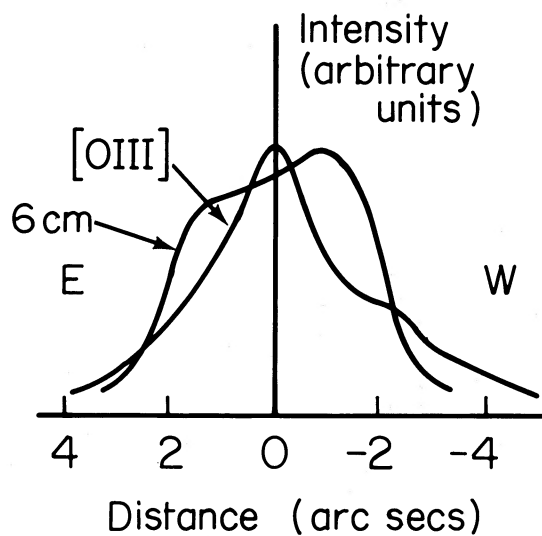


FIG. 8.—Profiles of the distribution of $[\text{O III}] \lambda 5007$ and 6 cm radiation in Mrk 573 with $1.6''$ resolution along their mutual major axis (P.A. = 117°). The profiles have been normalized to the same peak height and the central radio component assumed to coincide with the peak of optical continuum light. Note that the shoulders in the 6 cm distribution, which correspond to the outer radio components, are weaker in $[\text{O III}] \lambda 5007$.

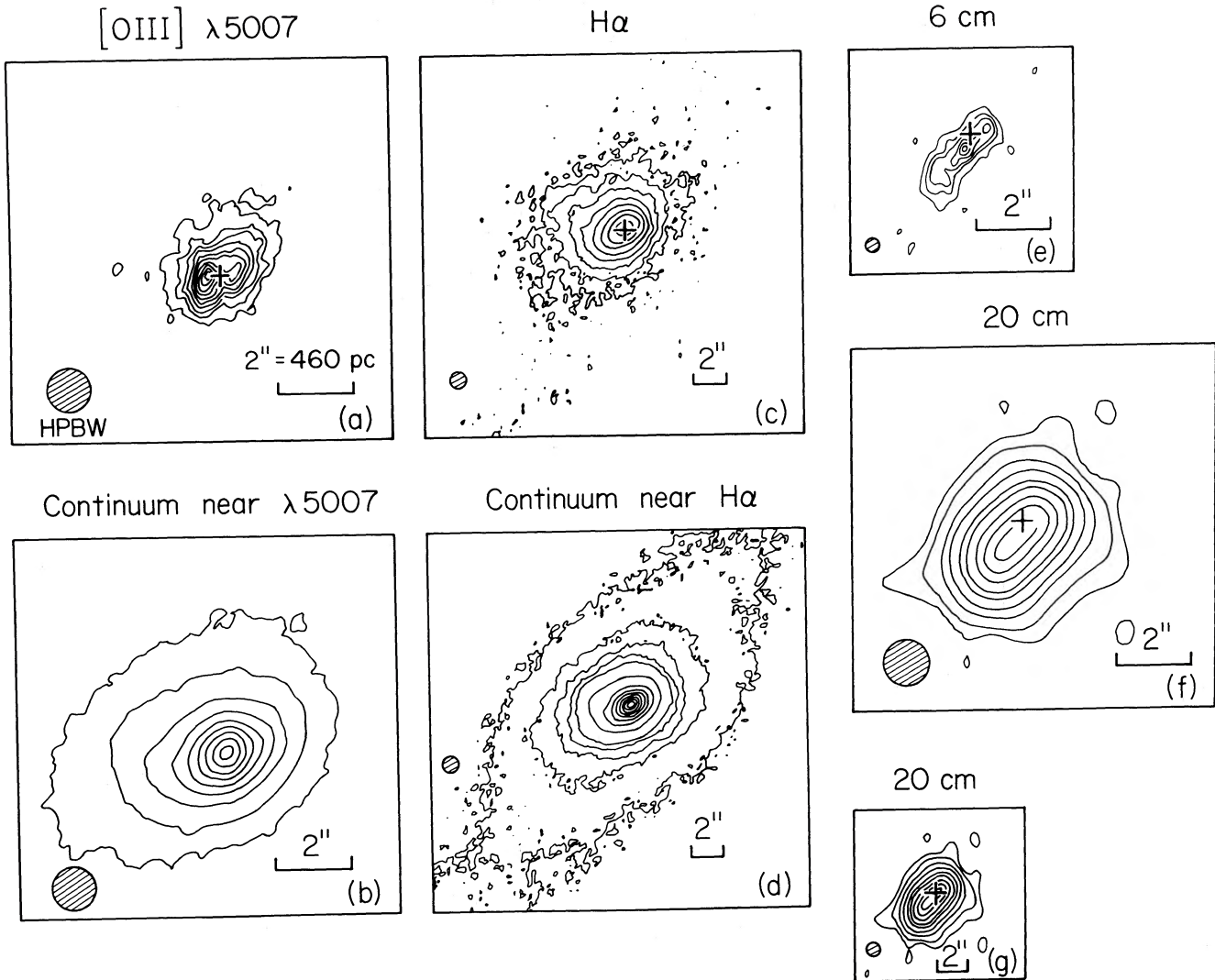


FIG. 9.—Mrk 1066, (a) [O III] $\lambda 5007$, contours at 50, 100, 150, 200, 250, 300, 350, 400, 450, and 500. (b) Continuum near $\lambda 5007$, contours at 100, 200, 400, 600, 800, 1000, 1200, 1400, and 1600. (c) $H\alpha$ contours at 60, 120, 240, 480, 960, 1920, 3840, and 7860. (d) Continuum near $H\alpha$, contours at 100, 200, 300, 400, 500, 1000, 2000, 3000, 4000, 5000, 6000, 7000, and 8000. (e) 6 cm VLA map with $0''.4$ resolution, contours at -10% , 10% , 20% , 30% , 50% , 70% , and 90% of the peak brightness of $3.9 \text{ mJy (beam area)}^{-1}$. (f) 20 cm VLA map with the same resolution ($1''.2$) and scale as (a) and (b); contours are plotted at -1% , 1% , 2% , 5% , 10% , 20% , 30% , 50% , 70% , and 90% of the peak brightness of $35.0 \text{ mJy (beam area)}^{-1}$. (g) As (f), but with the same resolution ($1''.0$) and scale as (c) and (d); contours are plotted at the same percentages as in (f), with the peak being $31.6 \text{ mJy (beam area)}^{-1}$.

Ulvestad and Wilson 1984b) are given in Figures 11c and 11d. The high-resolution 6 cm map (Fig. 11c) reveals a weak double source with separation $0''.4$ in P.A. = $78^\circ \pm 6^\circ$. After smoothing to the optical seeing ($1''.1$), this double becomes an elongated source with a (Gaussian deconvolved) FWHM $\approx 0''.7$. Thus the orientation and extent of the high-excitation emission line gas are essentially the same as those of the nuclear radio continuum radiation.

k) NGC 5135 (Seyfert Type 2, Fig. 12)

As for Mrk 270, the absence of reference stars precluded the formation of on-band minus off-band images for this object. Comparison of the on-band and off-band [O III] images (Figs. 12a and 12b) shows a clear difference, suggesting the [O III] emission is aligned N-S on the $\lesssim 2''$ scale, and possibly double. The $H\alpha$ on-band and off-band images (Figs. 12c and 12d) are also different, but any alignment of the gas is in the NE-SW

direction. Independent observations of NGC 5135 during the 1986 April–May run confirm the structures in these images.

Unpublished radio images (Ulvestad and Wilson 1988) are shown in Figures 12e–12g. The high-resolution map (Fig. 12e) shows a compact, bright region plus faint emission extending $\sim 6''$ to the NE (P.A. $\approx 30^\circ$). This is not, therefore, a typical double or triple structure, so classification as a “linear” radio source cannot be made. Figures 12f and 12g show the 6 cm data smoothed to typical seeings of $1''.0$ and $1''.5$, respectively. The radio source may broadly align with the $H\alpha$ emission.

We thank NATO for support under grant 675/83 and the Time Allocation Committee of the University of Hawaii for observing time on the 88 inch telescope. This research was also supported by NASA grant NAG8-529 to the University of Maryland. C. A. H. acknowledges the receipt of an S.E.R.C. studentship.

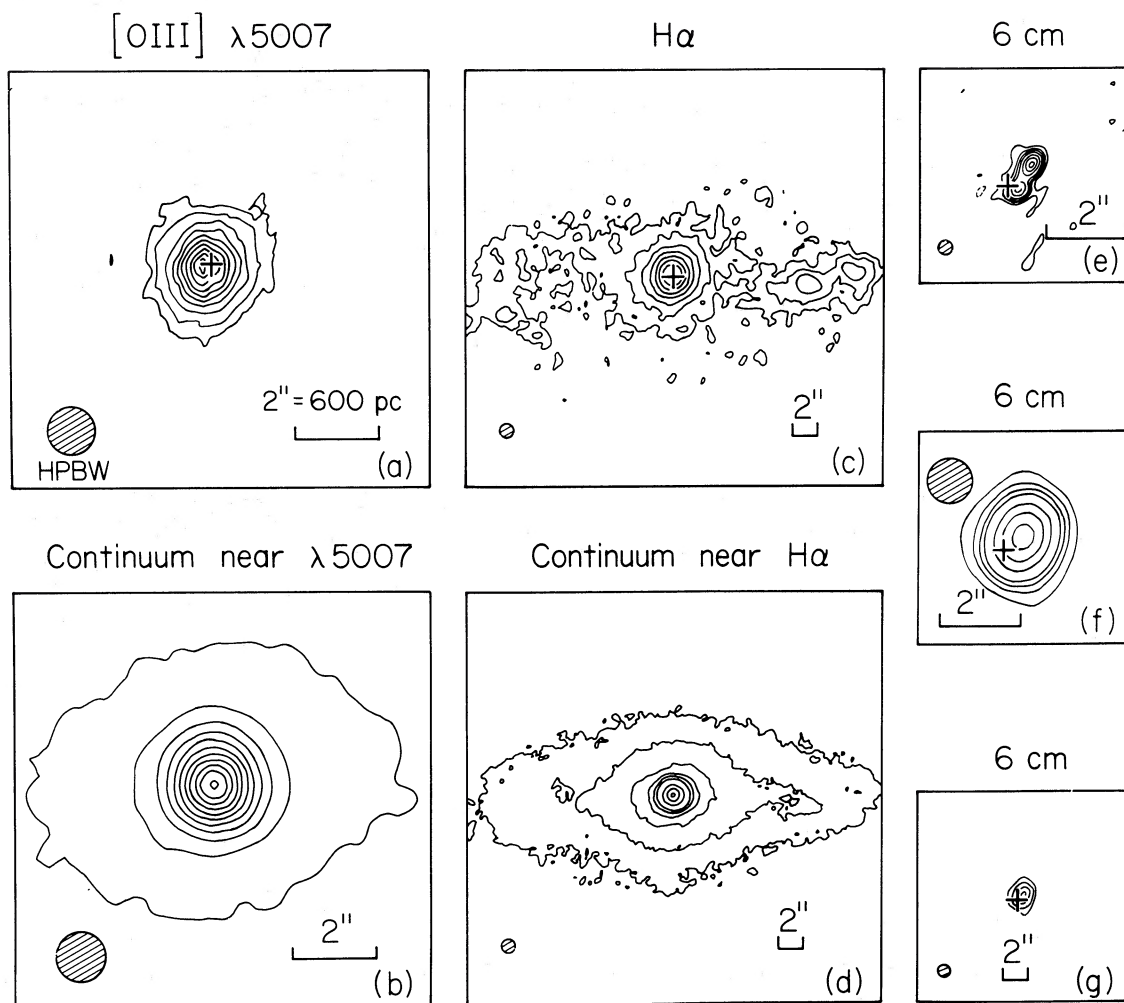


FIG. 10.—NGC 591 (= Mrk 1157). (a) $[O III] \lambda 5007$, contours at 50, 100, 200, 300, 400, 500, 600, 700, 800, and 900. (b) Continuum near $\lambda 5007$, contours at 100, 200, 300, 400, 500, 600, 700, 800, 900, 1000, and 1100. (c) $H\alpha$, contours at 50, 100, 200, 400, 800, 1600, and 3200. (d) Continuum near $H\alpha$, contours at 100, 200, 400, 600, 800, 1000, 2000, 3000, and 4000. (e) 6 cm VLAMAP with $0.4''$ resolution, contours at -7.5% , 7.5% , 15% , 22.5% , 30% , 50% , 70% , and 90% of the peak brightness of $3.5 \text{ mJy (beam area)}^{-1}$. (f) As (e), but with the same resolution ($1.2''$) and scale as (a) and (b); contours are plotted at the same percentages as (e), with the peak being $6.3 \text{ mJy (beam area)}^{-1}$. (g) As (e), but with the same resolution ($1.0''$) and scale as (c) and (d); contours are plotted at 5%, 15%, 50%, and 90% of the peak brightness of $5.7 \text{ mJy (beam area)}^{-1}$.

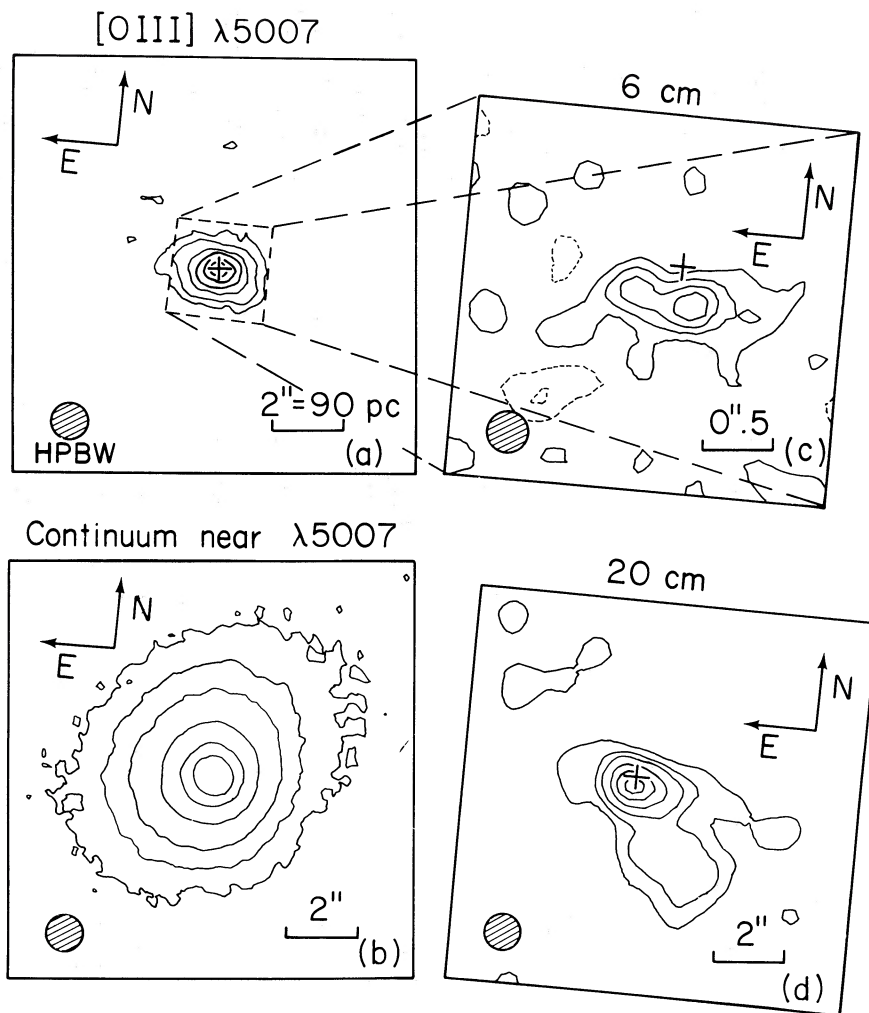


FIG. 11.—NGC 4051. (a) [O III] $\lambda 5007$, contours at 50, 100, 200, 300, 400, and 500. (b) Continuum near $\lambda 5007$, contours at 50, 100, 200, 500, 1000, and 1500. (c) 6 cm VLA map with resolution $0''.33$, contours are plotted at -40% , -20% , 20% , 40% , 60% , and 80% of the peak brightness of $0.76 \text{ mJy (beam area)}^{-1}$. (d) 20 cm VLA map with the same resolution ($1''.1$) and scale as (a) and (b); contours are plotted at -10% , 10% , 20% , 30% , 50% , 70% , and 90% of the peak brightness of $4.0 \text{ mJy (beam area)}^{-1}$.

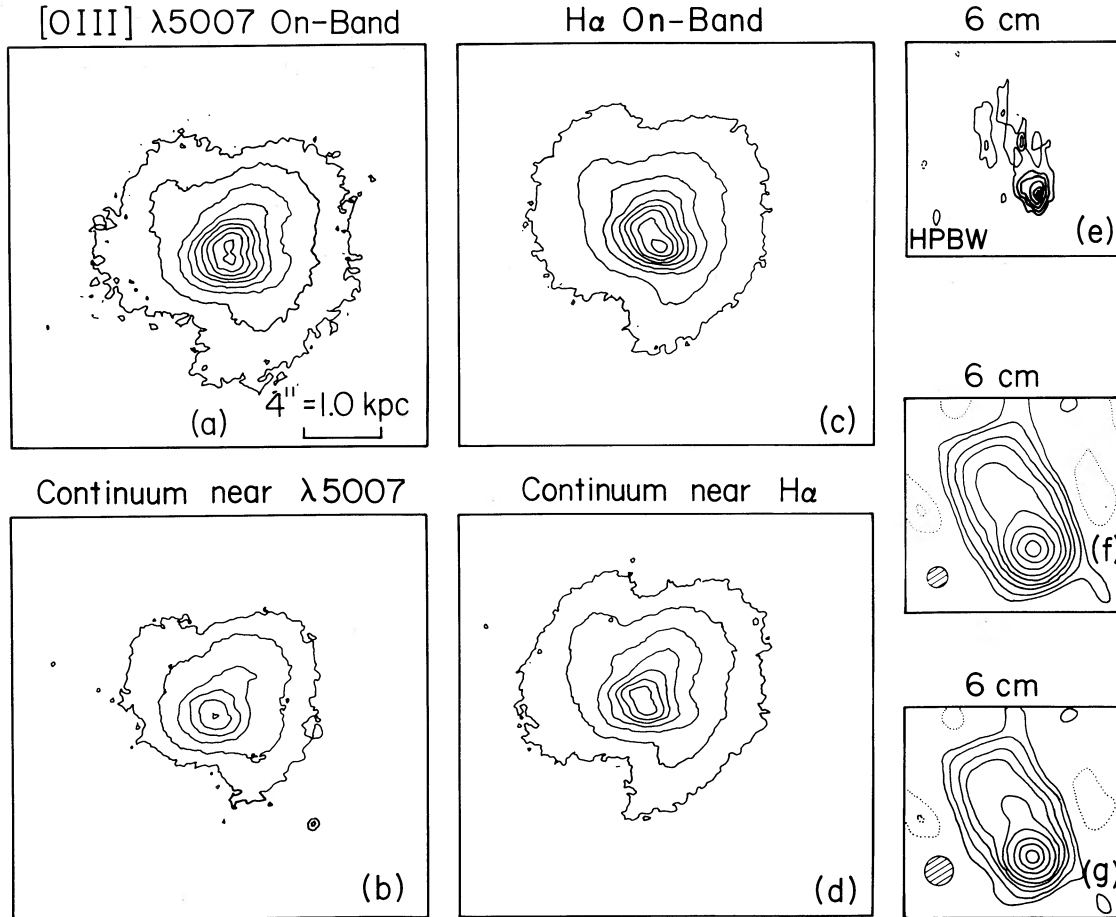


FIG. 12.—NGC 5135. (a) [O III] $\lambda 5007$ on-band (not continuum subtracted), contours at 100, 200, 400, 600, 800, 1000, 1200, 1400, and 1600. (b) Continuum near $\lambda 5007$, contours at 100, 200, 400, 600, 800, and 1000. (c) $H\alpha$ on-band (not continuum subtracted), contours at 200, 500, 1000, 1500, 2000, 2500, 3000, 3500, and 4000. (d) Continuum near $H\alpha$, contours at 200, 400, 800, 1200, 1600, 2000, and 2400. (e) 6 cm VLA map with resolution 0.3×0.7 , contours at -4% , 4% , 8% , 12% , 20% , 30% , 50% , 70% , and 90% of the peak brightness of $10.1 \text{ mJy (beam area)}^{-1}$. (f) As (e), but with a resolution of 1.0 and contours -4% , -2% , 2% , 4% , 8% , 12% , 20% , 30% , 50% , 70% , and 90% of the peak brightness of $19.0 \text{ mJy (beam area)}^{-1}$. (g) As (f), but with a resolution of 1.5 ; contours are plotted at the same percentages as in (f), with the peak brightness being $23.6 \text{ mJy (beam area)}^{-1}$.

REFERENCES

- Adams, T. F. 1973, *Ap. J.*, **179**, 417.
 Antonucci, R. R. J. 1983, *Nature*, **303**, 158.
 Boksenberg, A. 1977, in *IAU Colloquium 40, Astronomical Applications of Image Detectors with Linear Response*, ed. M. Duchesne and G. Lelièvre (Paris-Meudon) (Paper 13).
 Capriotti, E. R., and Foltz, C. B. 1982, *Ap. J.*, **255**, 48.
 Carroll, T. J., and Kwan, J. 1983, *Ap. J.*, **274**, 113.
 Clements, E. D. 1981, *M.N.R.A.S.*, **197**, 829.
 ———. 1983, *M.N.R.A.S.*, **204**, 811.
 Contini, M., and Aldrovandi, S. M. V. 1983, *Astr. Ap.*, **127**, 15.
 De Robertis, M. M. 1987, *Ap. J.*, **316**, 597.
 De Robertis, M. M., and Osterbrock, D. E. 1984, *Ap. J.*, **286**, 171.
 Feldman, F. R., Weedman, D. W., Balzano, V. A., and Ramsey, L. W. 1982, *Ap. J.*, **256**, 427.
 Ferland, G. J., and Osterbrock, D. E. 1986, *Ap. J.*, **300**, 658.
 Ferland, G. J., and Shields, G. A. 1985, in *Astrophysics of Active Galaxies and Quasi-Stellar Objects*, ed. J. S. Miller (Mill Valley, CA: University Science Books), p. 157.
 Filippenko, A. V. 1985, *Ap. J.*, **289**, 475.
 Filippenko, A. V., and Halpern, J. P. 1984, *Ap. J.*, **285**, 458.
 Heckman, T. M., Miley, G. K., and Green, R. F. 1984, *Ap. J.*, **281**, 525.
 Heckman, T. M., Miley, G. K., van Breugel, W. J. M., and Butcher, H. R. 1981, *Ap. J.*, **247**, 403.
 Koski, A. T. 1978, *Ap. J.*, **223**, 56.
 Krolik, J. H., and Vrtilik, J. M. 1984, *Ap. J.*, **279**, 521.
 Kwan, J., and Carroll, T. J. 1982, *Ap. J.*, **261**, 25.
 Miley, G. K., and Heckman, T. M. 1982, *Astr. Ap.*, **106**, 163.
 Osterbrock, D. E. 1981, *Ap. J.*, **246**, 696.
 Pedlar, A., Unger, S. W., and Booler, R. V. 1984, *M.N.R.A.S.*, **207**, 193.
 Penston, M. V., Fosbury, R. A. E., Boksenberg, A., Ward, M. J., and Wilson, A. S. 1984, *M.N.R.A.S.*, **208**, 347.
 Phillips, M. M., Charles, P. A., and Baldwin, J. A. 1983, *Ap. J.*, **266**, 485.
 Smith, M. D. 1984, *M.N.R.A.S.*, **209**, 913.
 Terlevich, R., and Melnick, J. 1985, *M.N.R.A.S.*, **213**, 841.
 Ulvestad, J. S., and Wilson, A. S. 1984a, *Ap. J.*, **278**, 544.
 ———. 1984b, *Ap. J.*, **285**, 439.
 ———. 1988, *Ap. J. Suppl.*, submitted.
 Ulvestad, J. S., Wilson, A. S., and Sramek, R. A. 1981, *Ap. J.*, **294**, 106.
 Vernon, M. P. 1981, *Astr. Ap.*, **100**, 12.
 Vrtilik, J. M., and Carleton, N. P. 1985, *Ap. J.*, **294**, 106.
 Whittle, M. 1985a, *M.N.R.A.S.*, **213**, 1.
 ———. 1985b, *M.N.R.A.S.*, **213**, 33.
 Whittle, M., Haniff, C. A., Ward, M. J., Meurs, E. J. A., Pedlar, A., Unger, S. W., Axon, D. J., and Harrison, B. A. 1986, *M.N.R.A.S.*, **222**, 189.
 Whittle, M., Pedlar, A., Meurs, E. J. A., Unger, S. W., Axon, D. J., and Ward, M. J. 1988, *Ap. J.*, **326**, 125.

Wilson, A. S., and Heckman, T. M. 1985, in *Astrophysics of Active Galaxies and Quasi-stellar Objects*, ed. J. S. Miller (Mill Valley, CA: University Science Books), p. 39.

Wilson, A. S., Pooley, G. G., Willis, A. G., and Clements, E. D. 1980, *Ap. J. (Letters)*, **237**, L61.

Wilson, A. S., Ward, M. J., and Haniff, C. A. 1988, *Ap. J.*, **334**, in press (Paper II).

CHRISTOPHER A. HANIFF: Institute of Astronomy, Madingley Road, Cambridge CB3 0HA, England, UK

MARTIN J. WARD: Astronomy Department, FM-20, University of Washington, Seattle, WA 98195

ANDREW S. WILSON: Astronomy Program, University of Maryland, College Park, MD 20742

HIGH-RESOLUTION EMISSION-LINE IMAGING OF SEYFERT GALAXIES. II. EVIDENCE FOR ANISOTROPIC IONIZING RADIATION

ANDREW S. WILSON

Astronomy Program, University of Maryland

MARTIN J. WARD

Department of Astronomy, University of Washington

AND

CHRISTOPHER A. HANIFF

Institute of Astronomy, Cambridge

Received 1988 January 25; accepted 1988 April 27

ABSTRACT

In the preceding paper, we describe a direct imaging survey of Seyfert galaxies with “linear” radio structures and find that the major axes and spatial scales of the circumnuclear emission-line gas are very similar to those of the radio continuum sources. In the present paper, the nature of this close connection between thermal and relativistic gases is assessed in detail. Models in which the kinetic energy of the radio jets or plasmoids powers shock waves, which ionize the gas, seem energetically feasible but disagree with the off-nuclear line intensity ratios. Ionization by relativistic electrons is negligible, but they may contribute to the heating of the gas. We favor a scenario in which the radio jets and plasmoids shock, accelerate, and compress ambient and entrained gas, but the dominant source of ionization is the nonstellar nuclear ultraviolet continuum. This ultraviolet source appears to be partially beamed along the axis of the radio jet. Photoionization by ultraviolet synchrotron radiation generated via shocks in the ejecta may also contribute, especially in Seyfert 2 galaxies.

A comparison between the number of ionizing photons, N_i , inferred by extrapolation of the directly observed continuum, and the number of ionizing photons, $N_{H\beta}$, required to generate the $H\beta$ emission has been made for six galaxies in our sample. In at least two galaxies, we find $N_i \ll N_{H\beta}$, suggesting that the gas is exposed to a higher ionizing flux than inferred from direct observations of the nucleus, and supporting the idea of partial beaming. Similarly, the energy in the continuum between 100 Å and 1 μm, if emitted isotropically, is inadequate to fuel the thermal nuclear infrared sources, implying that the radiating dust is heated by a more luminous optical-ultraviolet source. We speculate that the nuclear infrared emission of Seyfert 2 galaxies arises from dust in molecular clouds exposed to the partially beamed radiation, and we predict that the 10 μm sources should align with the radio axes. The partial beaming of the optical-ultraviolet radiation may arise through “shadowing” by a dense, obscuring torus, or it could reflect the intrinsic distribution of photons radiated by the accretion disk as a function of angular distance from its rotation axis (“polar diagram”).

Subject headings: galaxies: jets — galaxies: Seyfert — galaxies: structure — radio sources: general

I. INTRODUCTION

In the preceding paper (Haniff, Wilson, and Ward 1988, hereafter Paper I), a direct imaging survey of 11 Seyfert galaxies in the $H\alpha$ and [O III] $\lambda\lambda 4959, 5007$ emission lines is reported. The galaxies observed were chosen to contain “linear” radio sources (i.e., double, triple, or “jetlike” radio sources, straddling the optical continuum nucleus). However, the classification of the radio structure of one of them (NGC 5135) as “linear” is very doubtful, so we omit it from further discussion. The results of the survey of the remaining 10 may be summarized as follows:

1. The [O III] $\lambda\lambda 4959, 5007$ emission-line region is spatially resolved in all the galaxies. The amount of information in the emission-line distributions ranges from slight in galaxies with very compact ($\lesssim 0''.8$) radio doubles and emission-line regions (e.g., NGC 591 and NGC 4051) to detailed in galaxies with very extended narrow line regions (e.g., Mrk 78 and Mrk 573). In addition, $H\alpha$ is spatially extended in almost all the galaxies.

2. After smoothing VLA radio maps to the optical seeing, a comparison between emission-line and radio continuum dis-

tributions was possible. The position angles of the major axes of the [O III] and radio continuum images generally agree to within the errors of measurement (see col. [7], Table 2 of Paper I). These errors are large when the radio/emission-line region is compact, and in such cases (e.g., NGC 591) only an alignment in the same quadrant can be demonstrated. In most galaxies, however, the agreement of radio and emission-line axes is excellent, typically to better than $\pm 5^\circ$, which is within the measurement errors. There is also good agreement between radio and $H\alpha$ axes (col. [8], Table 2 of Paper I). Such alignment between the linear radio source and the high-excitation narrow-line region is now established in about 15 Seyfert galaxies (see Wilson 1987 for other examples).

3. The spatial extents of the radio doubles/triples and the bright inner regions of emission-line gas are very similar. The degree to which a comparison can be made depends, as above, on the angular extent. For compact regions, Gaussian deconvolutions from the effects of seeing and the radio beam show similar radio and emission-line FWHM (e.g., NGC 4051). For extended cases, detailed correspondences between the mor-

phologies are found. In Mrk 78, much of the [O III] emission is associated with the outer radio clouds. The distribution of [O III] appears to be double, straddling the optical continuum peak, and associated with the radio components in Mrk 34 and perhaps in Mrk 1066. The [O III] distribution in Mrk 573 shows a bright central core plus extended emission at the locations of the outer radio components. Association between high-excitation gas and radio lobes appears, therefore, to be a common property of Seyfert galaxies.

4. Examination of columns (9) and (10) of Table 2 in Paper I shows a possible tendency for the major axes of the optical continuum isophotes and the radio source to align when the position angle of the continuum isophotes refers to the same spatial scale as the radio source. The degree of alignment is, however, by no means as good as that between the radio and emission-line gases.

Section II is devoted to a discussion of the nature of the relationship between the radio continuum and optical emission-line distributions. This effect clearly indicates a close connection between the synchrotron-emitting relativistic particles and magnetic fields, and the thermal gas at $\sim 10^4$ K which is responsible for the emission lines. We discuss various possible physical processes which could be responsible and use arguments based on observational and simple energetic criteria to constrain them. In § III, we present comparisons between the number of ionizing photons inferred from the observed continua and the number inferred from the Balmer line fluxes, and also between the powers in the continuum available to heat dust and the thermal, nuclear infrared luminosities of the Seyfert 2's in our sample. The results tend to favor the idea that the optical-ultraviolet continua are not radiated isotropically. Conclusions are summarized in § IV.

II. NATURE OF THE RELATIONSHIP BETWEEN THE RADIO CONTINUUM AND EMISSION-LINE GASES

The connection between the relativistic and thermal gases could arise because either: (a) the kinetic energy of the ejected radio-emitting clouds is responsible for the heating and/or ionization of the line emitting gas; or (b) the thermal gas is ionized and/or heated by relativistic particles, the presence of which is indicated by the radio synchrotron radiation; or (c) the ejected radio plasma compresses ambient or entrained thermal gas, increasing the emissivity of the lines and rendering them more readily visible in the vicinity of the radio components than elsewhere, independent of the details of the heating and ionization; or (d) ionizing photons escape preferentially along the rotation axis of the disk which is presumed to collimate the radio ejecta, or one which is coplanar with it.

We discuss these possibilities in turn.

a) Kinetic Energy Models

A correlation between the monochromatic radio power at 1.4 GHz and the [O III] $\lambda 5007$ luminosity has been noted by a number of workers (de Bruyn and Wilson 1978; Phillips, Charles, and Baldwin 1983; Whittle 1985). Figure 1 is a related diagram in which the ratio of the integrated radio luminosity [$L(\text{radio})$] to the total emission-line luminosity of the narrow-line region [$L(\text{narrow lines})$] is plotted against $L(\text{narrow lines})$. The radio luminosity has been found by integrating the radio spectrum from 10 MHz to 100 GHz. The spectrum was taken to be of power-law form, $S \propto \nu^{-\alpha}$, with index α determined from flux density measurements at two or more centimetric wavelengths, if available. We used $\alpha = 0.75$ if the galaxy has

been detected at only one radio wavelength. For most galaxies plotted in Figure 1, detailed spectrophotometric observations are not available. By using the model calculations of optical and ultraviolet line intensities by Ferland and Osterbrock (1986), supplemented by Koski's (1978) measurements of lines not included in their Table 5, we estimate that the total power in line emission from the narrow line region is $L(\text{narrow lines}) \approx 14 L([\text{O III}] \lambda 5007)$ on average. This relationship has been used to derive all the line luminosities plotted in Figure 1, which contains all Seyfert galaxies with measurements of both [O III] $\lambda 5007$ and radio continuum fluxes. No corrections for obscuration were applied to the [O III] $\lambda 5007$ fluxes. As may be seen from Figure 1, the ratio $L(\text{radio})/L(\text{narrow lines})$ ranges between 10^{-2} and 10^{-4} for $L(\text{narrow lines})$ in the range 10^{40} – 10^{44} ergs s^{-1} . Allowance for obscuration would make the ratio even smaller.

If both the radio continuum and emission lines are powered solely by the kinetic energy of the same outflow, we may write

$$L(\text{radio}) = \epsilon_r L(\text{kinetic}),$$

and

$$L(\text{narrow lines}) = \epsilon_l L(\text{kinetic}),$$

where ϵ_r and ϵ_l are the efficiencies with which kinetic energy is converted into nonthermal radio and optical plus ultraviolet emission lines, respectively. From the data plotted in Figure 1, we have $\epsilon_r/\epsilon_l \approx 10^{-4}$ – 10^{-2} .

Generation of line emission in such a model would occur via thermalization of the outflow in shocks, with the value of ϵ_l depending on the shock properties. The power per unit area converted into heat in a strong shock is of order $\rho_{\text{no}} V_s^3/2$, where ρ_{no} is the preshock mass density and V_s is the shock velocity. An estimate of the emission efficiency is then $\epsilon_l \approx 2I(\text{narrow lines})/\rho_{\text{no}} V_s^3$, where $I(\text{narrow lines})$ is the sum of the intensities of the narrow lines per unit area of shock. Unfortunately, the appropriate values for ρ_{no} and V_s in the present context are unknown, and are likely to vary from galaxy to galaxy. As an illustration, we consider the emission-line spectra of plane radiative shocks with velocities in the range 40–200 km s^{-1} , typical preshock densities of 10 cm^3 and preshock magnetic fields of 1 μG , which have been calculated by Shull and McKee (1979) and Raymond (1979). For our purposes, such a range of parameters could apply to shocks driven into interstellar clouds by a lower density, high-velocity outflow, such as a radio jet or an expanding lobe. By summing the intensities of the optical and ultraviolet lines calculated by Shull and McKee (1979, their Tables 7 and 8), and adding estimates of the intensities of a few lines they did not include, ϵ_l may be obtained. We find $\epsilon_l \approx 0.2$ – 0.4 . Thus a scenario in which the line emission originates in such shocks and the radio emission is also powered by the flow would be energetically consistent with the data, if $L(\text{kinetic}) \gtrsim 10^{40}$ – 10^{44} ergs s^{-1} (see Fig. 1), $\epsilon_r \approx 0.2$ – 0.4 and $\epsilon_r \approx (10^{-4}$ – $10^{-2})\epsilon_l$. Shocks with much lower or much higher velocities would have smaller ϵ_l . A more extensive discussion is precluded by our ignorance of the shock parameters and the limited range of shock models currently available.

A serious difficulty for all shock models, however, concerns the ratios of the emission-line intensities. It has long been known that the (narrow) emission-line ratios in spatially unresolved spectra of Seyfert galaxies are indicative of photoionization by a power-law spectrum (e.g., Koski 1978; Ferland and Shields 1985). More recently, spatially resolved, low-dispersion

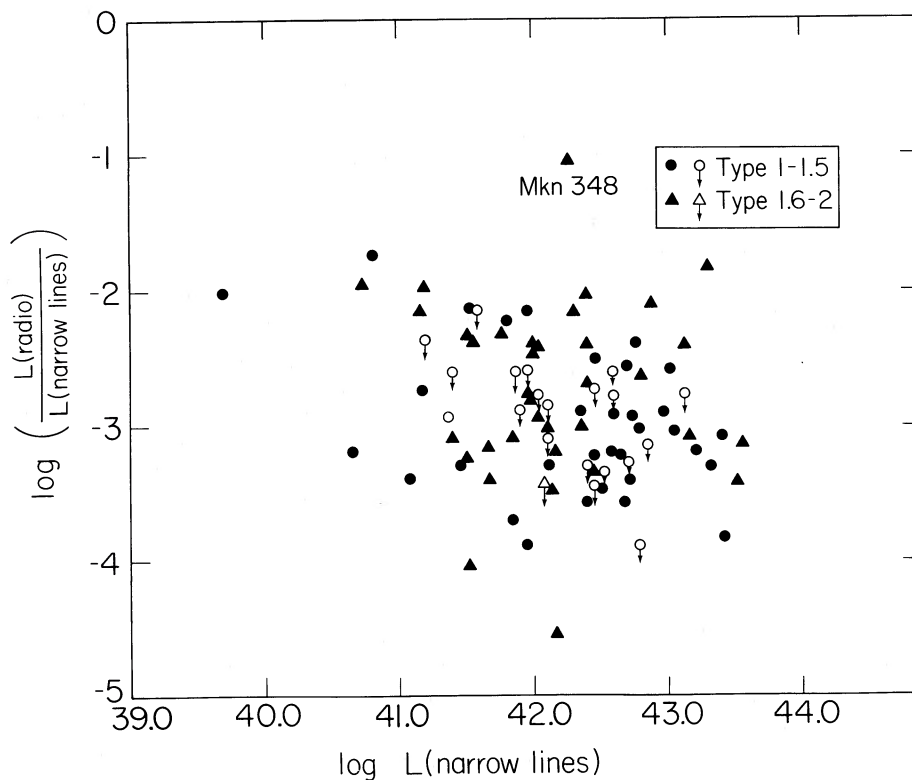


FIG. 1.—Plot of the ratio of the total radio luminosity, $L(\text{radio})$, to the total emission-line luminosity of the narrow-line region, $L(\text{narrow lines})$, against $L(\text{narrow lines})$. All Seyfert galaxies with measurements of both $[\text{O III}] \lambda 5007$ and radio continuum fluxes are plotted. Seyfert types 1–1.5 and 1.6–2 are plotted with different symbols. Open symbols represent upper limits. The radio luminosities were calculated from radio fluxes and spectral indices in de Bruyn and Wilson (1976), Wilson and Meurs (1982), Condon *et al.* (1982), Ulvestad and Wilson (1984*a, b*), Morris *et al.* (1985), Ulvestad (1986), Schommer *et al.* (1987), and Ulvestad and Wilson (1988). The emission-line luminosities were obtained as described in the text, using measurements of the flux of $[\text{O III}] \lambda 5007$ in Adams and Weedman (1975), Koski (1978), MacAlpine, Williams, and Lewis (1979), Yee (1980), Hawley and Phillips (1980), Osterbrock (1981), Shuder and Osterbrock (1981), Phillips and Malin (1982), Phillips, Charles, and Baldwin (1983), Goodrich and Osterbrock (1983), Ulvestad and Wilson (1983), and Penston *et al.* (1984).

spectra of a few galaxies with linear radio sources have been obtained (Balick and Heckman 1979; Wilson, Baldwin, and Ulvestad 1985), showing that the off-nuclear emission-line spectra are also characteristic of power-law photoionization. Whittle *et al.* (1988) have published medium-high dispersion long-slit spectra of the $H\beta$, $[\text{O III}] \lambda\lambda 4959, 5007$ region for 10 Seyferts with linear radio structures. They find that in the approximately seven cases where line-emitting components can be associated with the radio lobes, the flux ratios $F([\text{O III}] \lambda 5007)/F(H\beta) \approx 10\text{--}15$ for these components, which is very similar to the corresponding values for the nuclear components. These ratios are typical of power-law photoionized nebulae, and much higher than expected in steady flow, radiative shock wave models, even when shock velocities comparable to the emission line widths are considered (see Binette, Dopita, and Tuohy 1985 for models with shock velocities in the range $100\text{--}1000 \text{ km s}^{-1}$). It is noteworthy, however, that some finite age/optically thin shock models do exhibit $F([\text{O III}] \lambda 5007)/F(H\beta)$ ratios comparable to those observed (Binette, Dopita, and Tuohy 1985). Low-dispersion data including other lines (especially $[\text{O II}] \lambda 3727$) can distinguish such models from the power-law photoionized case.

Currently available data, then, favor the notion that the emission-line gas associated with the radio components is photoionized by a power-law continuum source. Such a source could either be located in the nucleus (see § II*d* below) or be associated with the radio lobes themselves. In the context of

kinetic energy models, the latter situation could arise if cosmic-ray electrons are accelerated *in situ*, presumably via shock waves in the flow, to energies capable of radiating ultraviolet synchrotron emission: $\gamma = E/mc^2 \approx 10^6\text{--}10^7$ for magnetic fields of $\sim 10^{-4} \text{ G}$. There is currently no evidence for such spatially extended, nonthermal sources of ionizing photons in Seyferts, but such a picture cannot be ruled out and might be attractive for Seyfert 2's, where the evidence for an ultracompact ionizing source is weaker than in Seyfert 1's. Searches with the Hubble Space Telescope for extended ultraviolet synchrotron sources in Seyfert galaxies would be very valuable. We emphasize that the above difficulties with the line ratios in "pure" shock wave models do not preclude scenarios in which the high-velocity gas in the narrow-line region is *accelerated* by the action of jets (Wilson 1982) or expanding radio lobes (Pedlar, Dyson, and Unger 1985; Wilson and Ulvestad 1987) on entrained or ambient interstellar gas. Shock waves are almost certainly present in and around the radio components and models including *both* their effects and those of photoionizing sources are clearly relevant (see Contini and Aldrovandi 1983).

b) Ionization and/or Heating by Relativistic Particles

The effects of heating and ionization by relativistic particles on the emission-line spectra of active galactic nuclei have been considered recently by Ferland and Mushotzky (1984), Cesar,

Aldrovandi, and Gruenwald (1985), and Gruenwald and Viegas-Aldrovandi (1987). By making a number of simplifying assumptions, Ferland and Mushotzky calculated the ratio of the rates of the relativistic electron (ξ) to photoelectric (Q) heat inputs as well as the ratio of the ionization rate by relativistic particles (Γ^*) to the ionization rate by conventional photoionization. Writing P_{rel} and P_{th} for the relativistic electron and thermal pressures, respectively, U for the ionization parameter [$U = Q(H)/4\pi N_e r^2 c$, with N_e the thermal electron density and r the separation between the ionizing source and the cloud in question), and β for the ratio of total heating by the cosmic rays to Coulomb heating (β takes into account collective effects; e.g., Scott *et al.* 1980], Ferland and Mushotzky's (1984) equations (9) and (10) may be written

$$\frac{\xi}{Q} = \frac{0.04\beta P_{\text{rel}}}{P_{\text{th}}},$$

and

$$\frac{\Gamma^*}{\Gamma} = \frac{10^{-8} P_{\text{rel}}}{U P_{\text{th}}}.$$

Here a temperature of 10^4 K has been adopted for the thermal gas. Photoionization models of the narrow-line region generally require an ionization parameter $U \approx 10^{-2}$ to reproduce the line ratios (e.g., Ferland 1981). If the relativistic electron and thermal pressures are comparable, as commonly appears to be the case in Seyferts (de Bruyn and Wilson 1978; Pedlar, Dyson, and Unger 1985; Unger *et al.* 1986), it is clear that the ionization rate by relativistic electrons is negligible in comparison with that by photons, as also concluded by Ulvestad (1981).

The relativistic electrons could be a significant source of heating, especially if collective effects are important. Ferland and Mushotzky (1984) studied the effect of the cosmic rays on the line ratios in a model of the narrow-line region with density $N = 10^3 \text{ cm}^{-3}$ and $U = 10^{-2}$. They found that the cosmic rays first affect the emission-line spectrum when $\beta P_{\text{rel}} \approx 10^{-9} \text{ ergs cm}^{-3}$, comparable to the thermal pressure. Therefore the detailed emission-line spectrum will be influenced by the presence of the cosmic rays, but they are probably not the dominant factor in defining the morphological correspondence between the radio and emission-line gases. As Ferland and Mushotzky (1984) note, there remain many theoretical uncertainties, such as the effect of the magnetic field in impeding the motion of cosmic rays into and through the emission-line clouds, the magnitude of collective effects and the densities of relativistic and subrelativistic protons, which cannot be inferred from the radio synchrotron spectrum. Further calculations of the effects of relativistic electrons on a photoionized gas would be valuable.

c) Compression of Thermal Gas by the Radio Ejecta

In its "purest" form, this scenario would attribute the alignment of the [O III] emission with the radio axis solely to *compression* of gas by the radio ejecta (and consequent enhancement of emission-line emissivity), even when the central ($\lesssim 1$ pc) photoionizing source radiates *isotropically*. As discussed above, the compression would presumably occur through the agency of radiative shock waves driven into entrained or ambient thermal material. Weak line emission would be expected from gas photoionized by the supposed isotropic nuclear source in directions away from the radio axis.

This picture accounts naturally for the identical *spatial scales* of the radio lobes and the high-velocity gas, but as there is now considerable evidence for anisotropic escape of ionizing photons from the inner nucleus (see below), we suspect that this mechanism is not wholly responsible for the observed relation between the radio and emission-line gases.

d) Anisotropic Escape of Ionizing Photons

In this picture, the emission-line gas is photoionized by a compact (≤ 1 pc) nuclear source, but the ionizing photons escape preferentially along the axis of the disk which also collimates the radio jet (e.g., Osterbrock 1983). We summarize here the evidence in favor of this point of view.

1. As noted above, off-nuclear optical spectroscopy often shows line ratios similar to the nuclear ones and characteristic of gas photoionized by a power law. Examples of such high ionization emission-line regions associated with linear radio sources in Seyfert galaxies include NGC 1068 (Balick and Heckman 1979; Baldwin, Wilson, and Whittle 1987), NGC 2110 (Wilson, Baldwin, and Ulvestad 1985), NGC 5643 (Morris *et al.* 1985), and NGC 5929 (Whittle *et al.* 1986).

2. In some cases, the nuclear nonstellar ultraviolet source, as estimated by extrapolation of the observed optical or ultraviolet continuum, apparently fails to provide enough ionizing photons to account for the recombination line emission. In NGC 1068, Baldwin, Wilson, and Whittle (1987) found this discrepancy to be a factor of at least 20, and perhaps as high as 200, for an off-nuclear cloud of high ionization gas apparently photoionized by the nucleus, while for gas in the nucleus itself, Neugebauer *et al.* (1980) claimed a factor of 6 discrepancy. A similar effect is probably present in NGC 2110 (Wilson, Baldwin, and Ulvestad 1985). Such discrepancies suggest the presence of sources of ionizing radiation which are invisible from Earth (perhaps because of obscuration) but which do shine out in some directions and illuminate the emission-line clouds (Neugebauer *et al.* 1980). One particular geometry involves the radiation escaping preferentially along the disk rotation axis, so the clouds in this direction are exposed to a much brighter ionizing flux than inferred via direct observations of the continuum from Earth. It is unclear whether this anisotropic photon escape, if it occurs, is an intrinsic property of the ionizing source, or whether it results from greater dust obscuration in the plane of the disk than along its rotation axis. The ionizing spectrum "seen" by an emission-line cloud a long way from a thin accretion disk is a function of the angular distance of the cloud from the disk's rotation axis (Netzer 1987), but it is doubtful whether the required degree of "collimation" can be produced in this way. The evidence that this possible deficit of ionizing photons in relation to the recombination line radiation is a common property of Seyfert 2 galaxies is discussed in depth in § III.

3. While NGC 1068 is traditionally classified as a Seyfert 2 galaxy, Antonucci and Miller (1985) have found that its optical polarized flux spectrum resembles the flux spectrum of a Seyfert 1 galaxy, with broad Balmer lines of $\text{FWZI} \approx 7500 \text{ km s}^{-1}$. They interpret their observations in terms of a torus of obscuring material surrounding the broad-line region and compact continuum source; these components can thus not be observed directly from Earth. The polarized continuum and broad emission lines result from the presence of a high-latitude gas of scattering particles, probably warm electrons, which partially scatter these radiations into our line of sight. The axis

of the torus required by the polarization observations is close to the direction of the radio jet.

4. Long-slit, high-dispersion spectra, oriented both along and perpendicular to the radio axes of a number of Seyfert galaxies, including some of those imaged in the present paper, have recently been obtained by Unger *et al.* (1987). These workers find high-excitation, very weak, narrow emission lines extending much further along the radio axis than perpendicular to it. Since the faint emission lines extend out well beyond the observed radio components, the kinetic energy and relativistic particles associated with the radio jets and lobes apparently play no role in ionizing or heating this gas. The gas is apparently normally rotating disk gas which has been photoionized by the nuclear source.

e) Summary

In summary, we feel that the gas associated with the radio lobes is almost certainly photoionized by a power-law, or similar, continuum source. This ultraviolet source could be located either *in situ*—i.e., within or near the lobes—or, more likely, in the compact ($\lesssim 1$ pc) nucleus itself. In the latter case, there is compelling evidence that the source does not emit isotropically, but is partially beamed along the radio axis. Such partial beaming can explain the alignment of radio and emission-line axes, but not the close agreement between the spatial extents of the radio and high-velocity thermal gas. An additional effect must be present, most likely compression of entrained or ambient thermal gas by the radio ejecta. The jet or expanding lobes drive radiative shocks into the gas, forming cool dense condensations, which are maintained in an ionized state by the ultraviolet source. It is possible, but less likely, that relativistic particles also contribute to the heating of the gas. High resolution emission-line imaging with the Hubble Space Telescope should define in finer detail the relationship between relativistic and thermal gases in Seyfert galaxies.

If the ultraviolet source is partially beamed along the radio axis, we expect that the number of ionizing photons estimated from the recombination line emission will, in most cases, be larger than that inferred directly from extrapolation of the observed optical-ultraviolet continuum. For the same reason there may also be discrepancies between the thermal infrared output and the observationally inferred number of optical-ultraviolet photons capable of heating dust to the required temperatures. In the next section we attempt a quantitative exploration of these questions for type 2 Seyfert galaxies.

III. IS THERE AN "ENERGY DEFICIT" IN SEYFERT 2 GALAXIES?

a) The Ionizing Continuum and the Recombination Line Emission

The method of estimating the number of ionizing continuum photons available and comparing this with the number required to produce the hydrogen line emission is, in principle, straightforward. Assuming radiative recombination under case B conditions, the relevant formulae are

$$N_{H\beta} = 2.1 \times 10^{52} (L_{H\beta}/10^{40} \text{ ergs s}^{-1}) \text{ photons s}^{-1},$$

where $N_{H\beta}$ is the number of ionizing photons necessary to produce an $H\beta$ luminosity $L_{H\beta}$, and

$$N_i = 4\pi D^2 C (\alpha h)^{-1} (v_1^{-\alpha} - v_2^{-\alpha}).$$

Here N_i is the number of photons in the continuum between v_1

and v_2 , D is the distance to the source, C is the constant in the flux density spectrum $F = Cv^{-\alpha}$, and h is Planck's constant. We take $v_1 = 3.3 \times 10^{15}$ Hz (912 Å) and $v_2 = 4.8 \times 10^{17}$ Hz (2 keV), noting that for the range of spectral indices considered here, N_i is insensitive to the exact choice of v_2 .

In practice a number of problems arise in estimation of the relevant parameters, which introduce uncertainties into the comparison of $N_{H\beta}$ and N_i :

1. Most of the ionizing photons are not directly observable. We shall assume a power-law form for the continuum, based on observations at optical, ultraviolet, and X-ray wavelengths. If Seyfert 2's were to have "big blue bumps," like those inferred for some Seyfert 1's and quasars, this method could result in a considerable underestimate of the number of ionizing photons.

2. The corrections for absorption and reddening are uncertain. In fact, these parameters need to be known along three different paths: (1) our line of sight to the ionizing continuum source, (2) our line of sight to the line-emitting gas, and (3) the path between the ionizing continuum source and the line-emitting gas. Estimates of (1) and (2) will be made from published observations, on a galaxy by galaxy basis. In the ultraviolet, we shall use the reddening law given by Code *et al.* (1976). We adopt $A_v = 0$ for path (3), since our philosophy is to make assumptions which minimize any apparent excess of $N_{H\beta}$ over N_i . If $A_v > 0$ for (3), the number of ionizing photons incident on the emission-line clouds will be reduced, thereby increasing any discrepancy.

3. Optical observations of the supposedly nonthermal continuum may be contaminated by stellar radiation. This problem is particularly pertinent to the few cases in which the nonthermal continuum is known in only the optical band.

4. The covering fraction of the ionized gas, as seen from the continuum source, is not known. A novel feature of our analysis is use of the emission-line images, when appropriate, to place upper limits on the covering fraction. These limits are again taken conservatively, with the philosophy of minimizing any calculated excess of $N_{H\beta}$ over N_i . Further, calculations indicate that the volume of gas needed to emit a certain power in a given line is much smaller than the overall volume occupied by the gas. The line-emitting gas is thus concentrated in condensations or cloudlets, with a small filling factor, and probably intercepts only a small fraction of the ionizing continuum. The magnitude of this covering factor is unknown and, in accord with our conservative approach, we have not included it in the calculations. Allowing for a small covering factor, due to the gas being confined to cloudlets, would greatly amplify any calculated excess of $N_{H\beta}$ over N_i .

We have restricted our calculations to the Seyfert 2 galaxies for which observations were described in Paper I, plus NGC 1068. In addition, we required at least two of the following four observational parameters to be known: the nonstellar optical flux at some wavelength, the slope of the optical nonstellar continuum, an ultraviolet flux, and a soft X-ray flux. Because of a lack of such information, Mrk 1066, NGC 591, and NGC 5135 are omitted from the discussion. Our results for the other galaxies are summarized in Table 1.

Markarian 3.—Malkan and Oke (1983) derived reddenings of $E_{B-V} = 0.27$ mag for the emission lines and $E_{B-V} = 0.50$ mag for the nuclear continuum of this galaxy. We have, therefore, performed the comparison between $N_{H\beta}$ and N_i for both $A_v = 0.8$ mag and 1.5 mag. The flux of the nonstellar optical continuum at 5500 Å, its spectral index α , and the $H\beta$ flux were also taken from Malkan and Oke (1983). These authors also

TABLE 1
THE NUMBER OF IONIZING PHOTONS INFERRED FROM THE CONTINUA AND THE NUMBER REQUIRED TO PRODUCE THE $H\beta$ EMISSION LINES^a

Galaxy	α	$\log C$	$\log N_i$	$\log N_{H\beta}$	$A_v(\text{mag})$	$N_{H\beta}/N_i$	Method for Power Law
Mrk 3	1.30	-6.84	52.62	53.76	0.8(1 & c)	14	Optical slope
	1.00	-10.83	53.40	54.09	1.5(1 & c)	5	Optical slope
	1.00	-10.83	53.40	53.76	{0.8(1)} {1.5(c)}	2.3	Optical slope
Mrk 34	1.51	-3.78	<53.42	53.59	0(1 & c)	>1.5	Opt. point plus X-ray limit
	1.51	-3.78	<53.42	54.10	{1.1(1)} {0(c)}	>5	Opt. point plus X-ray limit
Mrk 78	1.77	0.13	{52.08(E) 51.81(W)}	{52.91(E) 52.66(W)}	0(1 & c)	{6(E) 7(W)}	Ultraviolet spectrum
	1.77	0.13	{52.08(E) 51.81(W)}	{53.39(E) 53.15(W)}	{1.05(1)} {0(c)}	{20(E) 22(W)}	Ultraviolet spectrum
	1.16	-8.05	{53.54(E) 53.27(W)}	{53.39(E) 53.15(W)}	1.05(1 & c)	{0.7(E) 0.8(W)}	Ultraviolet spectrum
Mrk 270	1.54	-3.43	<51.90	51.86	0(1 & c)	>0.9	Opt. point plus X-ray limit
	1.54	-3.43	<51.90	52.23	{0.8(1)} {0(c)}	>2	Opt. point plus X-ray limit
Mrk 573	1.12	-10.17	52.32	52.62	0(1 & c)	2.0	Extrapolation optical plus X-ray point
	1.0	-11.08	53.32	53.08	1.0(1 & c)	0.6	Extrapolation optical plus X-ray point
NGC 1068	1.10	-8.39	52.91	52.89	0.3(1 & c)	1.0	Optical slope
	0.90	-10.94	53.55	53.16	0.9(1 & c)	0.4	Optical slope
	1.55	-1.64	52.71	52.74	0(1 & c)	1.1	Ultraviolet spectrum

^a Columns give the galaxy name, the spectral index, α , and normalization, C , of the continuum ($F_\nu = C\nu^{-\alpha}$), the number of ionizing photons available in the continuum, N_i , the number of ionizing photons required to produce the observed $H\beta$ flux, $N_{H\beta}$, the ratio $N_{H\beta}/N_i$, the visual absorption assumed, A_v , followed in parenthesis by 1 if the value of A_v was applied to $H\beta$ and by c if it was applied to the continuum, and the method used to define the continuum power law (see text). All values of N_i , except those for Mrk 78 (see text), assume a 100% covering factor by the ionized gas.

obtained a continuum spectrum with *IUE*, but the data are too noisy to provide a useful constraint on the spectrum.

Using a covering factor of 100% and the lower value of the reddening for both line and continuum, we find there are too few ionizing photons to produce the appropriately dereddened $H\beta$ luminosity by more than a factor of 10 (Table 1). When the power law used in this calculation is extrapolated to 2 keV, it predicts a flux that is somewhat higher than the X-ray measurement, but within a factor of 2 of it. Using the same assumptions and the higher value of the reddening, the deficiency of ionizing photons is reduced to a factor of ~ 5 . The extrapolation of the power law to 2 keV in this case predicts a flux too high by a factor of 40. If, following Malkan and Oke (1983), we adopt $A_v = 0.8$ mag for the lines and $A_v = 1.5$ mag for the nonstellar continuum, the discrepancy is only a factor of ~ 2 .

In view of the elongated form of the [O III] nebulosity and its alignment with the radio axis, we may assume a covering factor for the narrow-line region of $\lesssim 100\%$, but a precise value is hard to obtain (cf. Fig. 1 of Paper I). Conservatively speaking $\lesssim 50\%$ seems reasonable which would increase all the above numbers by a factor of 2. While all the numbers are subject to considerable uncertainty, there does seem to be some discrepancy between the extrapolated, observed continuum and the number of ionizing photons required to power $H\beta$ in Mrk 3. This conclusion would be firm if the line emission has the same morphology as the radio source (Fig. 1e of Paper I).

Markarian 34.—Considerably less information is available for this galaxy than for Mrk 3. For the continuum, we have used an estimate of the optical nonstellar continuum together with an upper limit to the X-ray flux, both from Kriss, Canizares, and Ricker (1980). This procedure estimates the maximum number of ionizing photons if the entire optical to

X-ray spectrum is a power law and its reddening zero. The $H\beta$ flux has been taken from Koski (1978), whose measurements were generally made through a $2.7 \times 4''$ aperture. If emission-line gas extends over a larger area, the value of $N_{H\beta}$ will be underestimated, and any excess of $N_{H\beta}$ over N_i reduced. For the case of no reddening, there are $\sim 50\%$ too few ionizing photons, an insignificant difference. If the $H\beta$ flux (but not the continuum) is dereddened using the observed Balmer decrement (Koski 1978), with an assumed intrinsically case B decrement, the discrepancy is a factor of ~ 5 . As for Mrk 3, the linear, possibly double, narrow-line region certainly reduces the covering factor below 100%, perhaps to $\lesssim 40\%$ (see Fig. 3c of Paper I), or to $\sim 5\%$ if the emission-line gas is concentrated in the radio lobes (Fig. 3e of Paper I). While this effect tends to increase the above small discrepancies, a definite conclusion cannot be drawn in the absence of information on the ultraviolet spectrum and its reddening.

Markarian 78.—For this object, we extrapolate the *IUE* spectrum to estimate the number of ionizing photons. The continuum fluxes at 2500 Å (Ferland and Osterbrock 1986) and at 1450 Å (Wu, Boggess, and Gull 1983) imply $\alpha = 1.77$ and $\log N_i = 53.04$. Extrapolation of this spectrum to 2 keV gives an X-ray flux within a factor of 2 of that observed (Kriss, Canizares, and Ricker 1980). Using the [O III] image, we estimate that the emission-line regions to the east and west of the nucleus subtend $\sim 11\%$ and 6% , respectively, of all sky at the nucleus. These covering factors are upper limits and will be smaller if either the line-emitting gas is actually in condensations with a small filling factor (see above) or the gas is concentrated within the off-nuclear radio components (Fig. 4e of Paper I). If the ionizing continuum source is compact, located at the optical continuum peak and radiates iso-

tropically, we obtain the values of N_i available for the east and west components separately (Table 1). The short time scale variability in the soft X-rays from Mrk 78 (Urry *et al.* 1986) provides support for our assumption that the ultraviolet source is compact. Taking the total $H\beta$ flux given by Koski (1978) and assuming a uniform $[O III] \lambda 5007/H\beta$ ratio (Whittle *et al.* 1988), the values of $N_{H\beta}$ can be calculated separately for the two components (Table 1). Comparison of N_i and $N_{H\beta}$ then indicates a deficit in the number of ionizing photons available by a factor of ~ 7 for both east and west components.

The above calculations assume $A_v = 0$ for both the line and continuum fluxes. Ferland and Osterbrock (1986) deduced $A_v = 1.05$ mag for the emission lines. If this correction is applied to $H\beta$ but not to the continuum, the discrepancies become 20 (east component) and 22 (west component); see Table 1. Ferland and Osterbrock (1986) considered that the ultraviolet continuum of Mrk 78 suffers little reddening, so the data strongly favor these last discrepancies. As an illustration, however, we consider the consequences of assuming that the *IUE* continuum is reddened by the same amount as the emission lines and then extrapolate it to determine N_i . In this case, there are sufficient ionizing photons (Table 1). However, such a continuum is most improbable, for an extrapolation predicts ~ 230 times the X-ray flux observed at 2 keV. We conclude that the model with $A_v(\text{lines}) = 1.05$ mag and $A_v(\text{cont}) \approx 0$ is the most plausible, so that the deficit between the number of ionizing photons needed to power the $H\beta$ line and the number available from the continuum is a factor of ~ 20 . We reemphasize that this conclusion results from the assumptions that the ultraviolet source is compact, associated with the optical nucleus and radiates isotropically.

Markarian 270.—The data on this galaxy are quite limited, so we follow the same procedure as for Mrk 34. The continuum is defined by the nonstellar flux at 4400 Å and the upper limit to the X-ray flux at 2 keV (Kriss, Canizares, and Ricker 1980). The $H\beta$ flux is taken from Koski (1978). For zero reddening, N_i and $N_{H\beta}$ are essentially equal. If the reddening inferred from the Balmer line decrement is applied to $H\beta$, but not to the continuum, the discrepancy is a factor of 2 (Table 1). This difference is insignificant in view of our ignorance about the ultraviolet continuum of Mrk 270.

Markarian 573.—The sources for the $H\beta$ line strength are Koski (1978) and Ulvestad and Wilson (1983), and we have averaged their measurements. Koski has also estimated the nonstellar fraction of light in the continuum at the wavelength of $H\beta$. This continuum has been extrapolated by Ferland and Osterbrock (1986) to derive a flux at 2500 Å. Joining this last flux to the soft X-ray point (Ulvestad and Wilson 1983) with a power-law spectrum, and making no reddening correction, we find that there are about half the ionizing photons required to account for the $H\beta$ luminosity (Table 1). As an illustration of the effects of reddening, we have dereddened the $H\beta$ and 2500 Å continuum fluxes by $A_v = 1.0$ mag (as implied by the Balmer decrement; Koski 1978) and extrapolated the continuum to shorter wavelengths, arbitrarily assuming $\alpha = 1.0$. The result is that the ionizing continuum contains 1.7 times as many photons as required to power $H\beta$ (Table 1). However, this continuum may be too bright, since its extrapolation to soft X-rays gives a flux 18 times too high. Thus, the lack of ultraviolet continuum information precludes a conclusion if the covering factor is 100%. The $[O III]$ image is highly elongated (Fig. 7a of Paper I), suggesting a small covering factor, although a substantial part of the flux is contained in an unresolved source coincident with the nucleus.

NGC 1068.—This galaxy is not included in our imaging sample, but we make the photon balance calculation because detailed observations are available, and to serve as a comparison. We follow Malkan and Oke (1983) and consider two possible continuum forms. The first is appropriate to $A_v = 0.3$ and has $\alpha = 1.1$, and the second to $A_v = 0.9$ with $\alpha = 0.9$. Once again, the consistency of such continua can be checked by extrapolation to the X-ray region [$F_x(2 \text{ keV}) \approx 4.8 \times 10^{-30}$ ergs $\text{cm}^{-2} \text{ s}^{-1} \text{ Hz}^{-1}$; Monier and Halpern 1987]. For the first continuum form (lower reddening), near equality between N_i and $N_{H\beta}$ ($H\beta$ flux from Koski 1978) is found (Table 1). However, the extrapolation to 2 keV provides ~ 30 times the observed flux. For the second continuum form (higher reddening), $N_i = 2.5 N_{H\beta}$ (Table 1), but the extrapolation to 2 keV provides ~ 300 times the observed flux. These spectra are almost certainly too flat, and, as an alternative, we use the ultraviolet spectrum favored by Monier and Halpern (1987), which has $\alpha = 1.55$. This spectrum gives $N_i \approx N_{H\beta}$ and its extrapolation to 2 keV agrees with the observed flux to within a factor of 2. Our conclusion is that for a 100% covering factor of the ionized gas, there is no discrepancy between N_i and $N_{H\beta}$ for the nuclear source in NGC 1068. The difference between this conclusion and that of Neugebauer *et al.* (1980) is indicative of the uncertainty in the intrinsic spectrum of the ionizing photons.

The circumnuclear, high-velocity line-emitting gas in NGC 1068 lines up with the radio source (Walker 1968; Wilson and Ulvestad 1982; Cecil, Tully, and Bland 1986), so a covering factor $\ll 100\%$ is likely. Also, the gas is likely to be clumped. Further, Baldwin, Wilson, and Whittle (1987) have shown that for a region of high-ionization gas some 20" from the nucleus along the radio axis, there are too few nuclear ionizing photons (by a factor of 20–200), if the ultraviolet radiation is radiated isotropically. These arguments favor partial beaming of the ultraviolet radiation along the radio axis.

b) *The Dust-Heating Continuum and the Thermal Infrared Emission*

Dust absorbs energy efficiently between ~ 100 Å and $1 \mu\text{m}$ and emits between 1 and $100 \mu\text{m}$ (Carleton *et al.* 1987). A natural model for the nuclear infrared emission of Seyfert 2's is one in which dust grains are heated by radiation in the former band and reradiated in the latter. In principle, a straightforward comparison between the powers available in the two bands can check whether the dust "sees" the same $100 \text{ Å} - 1 \mu\text{m}$ continuum as we infer from direct observation. If the inferred power (L_H) in the $100 \text{ Å} - 1 \mu\text{m}$ band is equal to or greater than the $1 - 100 \mu\text{m}$ power (L_{IR}), a model in which both bands are emitted isotropically would be consistent with the data. On the other hand, if there is a deficiency of dust heating in comparison with dust radiated power, we must infer that either there are extra sources of $100 \text{ Å} - 1 \mu\text{m}$ radiation which heat the dust but are hidden from our view, or that the $100 \text{ Å} - 1 \mu\text{m}$ radiation is not emitted isotropically. A special case of the former situation would be a single, totally obscured, dust-heating source. In view of the evidence (§ IIIa) for partial beaming of the ionizing radiation, it seems worthwhile to explore whether the same may be true of the band which heats the dust.

In practice, two complications arise. First, the *IRAS* fluxes reflect the sum of the emission from the nucleus and the galaxy. Second, there is potentially a direct contribution to the infrared emission from the low-frequency extension of the optical-ultraviolet power law. We restrict our discussion to four of the six galaxies discussed in § IIIa: Mrk 3, Mrk 78, Mrk 573, and

NGC 1068. The other two, Mrk 34 and Mrk 270, do not have sufficient multifrequency data available to justify detailed calculations.

There are both qualitative and quantitative ways of estimating the ratio of nuclear to nonnuclear infrared emission. All the objects discussed here have *warm IRAS* colors, with the energy distribution ($\log \nu f_\nu$ vs. $\log \nu$), peaking around $\log \nu \approx 13$ ($\lambda \approx 30 \mu\text{m}$). This suggests that the infrared emission is dominated by nuclear activity rather than cooler normal bulge or disk emission. Quantitatively, we can compare the ground-based small-aperture measurements at 10 and 20 μm with the much larger aperture *IRAS* measurements at 12 and 25 μm . For Mrk 3, we find that about half the total emission at 10 and 20 μm originates from inside 8".5. This ratio need not be the same for the flux at 60 and 100 μm , but since the peak occurs at 30 μm , a correction of a factor 2 would be appropriate to estimate the nuclear component of the *IRAS* fluxes. For NGC 1068, there is a similar difference between the *IRAS* 12 and 25 μm measurements and those at 10 and 20 μm through an 8".5 ground-based aperture. Indeed, Telesco *et al.* (1984) have shown that half of the total infrared luminosity from NGC 1068 is associated with the Seyfert nucleus and half with the starburst disk. We have, therefore, estimated the nuclear infrared luminosity (L_{IR}) for all four galaxies by dividing the total infrared luminosity by a factor of 2.

For Mrk 3, Mrk 573, and NGC 1068, the contribution of the optical-ultraviolet power law (Table 1) to the infrared luminosity is negligible. For Mrk 78, the low-frequency extension of the ultraviolet power law appropriate to $A_v = 0$ could dominate the infrared light if it extended to 30 μm . However, this is clearly not the case, since the *IRAS* spectrum of this galaxy is dominated by a strong peak near 30 μm , which is totally inconsistent with significant emission from the power law. Any direct contribution of the optical-ultraviolet power law to the infrared emission has, therefore, been neglected in all four objects.

The results are summarized in Table 2, where L_{H} has been obtained by integrating the continua given in Table 1 for the specified value of A_v from 100 \AA to 1 μm . The only case with $L_{\text{H}} > L_{\text{IR}}$ is Mrk 78, when $A_v = 1.05$ mag is assumed. As discussed in § IIIa, this value of A_v is actually derived from the emission lines, and it is most unlikely that the ultraviolet continuum of Mrk 78 is reddened by this amount (Ferland and Osterbrock 1986). In all other cases, $L_{\text{H}} < L_{\text{IR}}$, the deficit ranging from a factor of 2.2 to 19. In general, these results tend to support a model in which the dust radiating the nuclear infrared emission is heated by a continuum with intrinsically more power than is inferred from direct observations of the nucleus. One particular model with these properties is one in which the *dust-heating continuum, like the ionizing continuum, is partially beamed along the radio axis*. We may envisage dense molecular clouds, lying along or near the radio axis, being exposed to this luminous heating source, and their warm dust dominating the nuclear infrared output. A prediction of this model is that the mid-infrared sources in Seyfert galaxies with linear radio sources should align with their radio axes. There is already evidence that this may be the case in NGC 1068. Tresch-Fienberg *et al.* (1987) have resolved the 10 μm nuclear source in this galaxy into two components, one associated with a weak radio peak in the jet and the other with the nucleus. These authors note several difficulties with the idea that the off-nuclear source originates from dust heated by the nuclear continuum. However, at least some of the problems may be overcome in our scenario, in which the continuum responsible

TABLE 2
THE INFRARED LUMINOSITY AND THE DUST-HEATING
ENERGY AVAILABLE IN THE CONTINUUM^a

Galaxy	A_v	$\log L_{\text{IR}}$	$\log L_{\text{H}}$	$L_{\text{IR}}/L_{\text{H}}$
Mrk 3	0.8	43.94	42.79	14
Mrk 3	1.5	43.94	43.41	3.4
Mrk 78	0	44.25	43.53	5.2
Mrk 78	1.05	44.25	44.59	0.46
Mrk 573	0	43.67	42.39	19
Mrk 573	1.0	43.67	43.33	2.2
NGC 1068	0	44.21	43.03	15
NGC 1068	0.3	44.21	43.14	12
NGC 1068	0.9	44.21	43.68	3.4

^a Columns give the galaxy name, the assumed A_v (in magnitudes), the observed infrared luminosity, L_{IR} , the power available to heat the dust, L_{H} (both in ergs s^{-1}), and the ratio $L_{\text{IR}}/L_{\text{H}}$. The spectrum assumed to calculate L_{H} is identified by the value of A_v and Table 1. All the observed values of L_{IR} have been reduced by a factor of 2 to set more realistic limits on the nuclear thermal component (see text).

for heating the dust is much more luminous than direct observations of the nucleus indicate. If this picture is correct, we expect the nuclear source as well will line up with the radio axis when adequate spatial resolution becomes available in the mid-infrared. This source might, for example, be connected with the 0".7 scale radio triple in NGC 1068 (Ulvestad, Neff, and Wilson 1987). Our view differs from that of Krolik and Begelman (1988), who ascribe the nuclear infrared emission to warm dust in the obscuring torus which was invoked by Antonucci and Miller (1985) to account for their polarization observations.

IV. CONCLUSIONS

The principal conclusions of this paper and Paper I are as follows:

1. In Seyfert galaxies containing double, triple, or jetlike radio sources, there is an excellent correspondence between the major axes of the radio source and the high-velocity, emission-line gas (narrow line region).
2. The spatial extents of the relativistic and thermal gases are very similar, and typically of order several hundred parsecs. In at least three cases, there is strong evidence that the [O III] image has a double structure associated with the outer radio components.
3. Shock waves or relativistic particles are probably not the dominant source of ionization of the off-nuclear thermal gas. Rather, this gas is almost certainly photoionized by a continuum source with a power-law, or similar, spectrum.
4. The ultraviolet continuum source probably resides in the compact ($\lesssim 1$ pc) nucleus, but the ionizing radiation appears to be partially beamed along the radio axis. This last conclusion is favored by the morphology of the ionized gas and by an intercomparison of the number of ionizing photons calculated by extrapolation of the observed optical, ultraviolet, or X-ray continuum (N_i) and the number required to power the narrow-line H β emission by radiative recombination ($N_{\text{H}\beta}$). We find $N_i \ll N_{\text{H}\beta}$ in at least two type 2 Seyferts, suggesting that the gas is exposed to a higher intensity of ionizing continuum radiation than is observed along our line of sight to the nucleus. The solid angle of the cone into which the ionizing photons are

“beamed” would be expected to be wavelength-dependent if the anisotropy is an intrinsic property of the accretion disk. Direct, high-resolution images in different emission lines covering a range of ionization potential and critical density could be used, in conjunction with a photoionization model, to map out the variations of both the intensity of ionizing radiation and the thermal gas density as a function of distance along and from the cone's axis. Such work would provide very direct constraints on the properties of the central ionizing source. Ultraviolet photons generated *in situ* by synchrotron radiation within the jet are another potential source of ionization.

5. A comparison between the power in the optical-ultraviolet continuum available to heat dust (L_H) and the thermal luminosity of the nuclear infrared source (L_{IR}) shows $L_{IR}/L_H \approx 2-20$ in four type 2 Seyfert galaxies with linear radio structure. This result suggests that more radiation is available to heat the dust than escapes from the nucleus along our line of sight. As for the ionizing radiation, one possibility is preferential escape of part of the $100 \text{ \AA} - 1 \text{ \mu m}$ continuum along the radio axis. The nuclear infrared emission of Seyfert 2 galaxies

would then arise from dust in molecular clouds heated by this beamed ultraviolet radiation. If so, the thermal 10 \mu m sources in Seyfert 2 galaxies should align with their radio axes. The well-known correlation between radio and infrared luminosities in Seyfert galaxies would then reflect a relation between the power in the jet and the power in the partially beamed ultraviolet light which heats the dust.

6. There is a possible broad trend (requiring further observations for confirmation) for the radio axes to align with the optical continuum axes on a similar spatial scale. This optical light could originate either in compact stellar barlike features or be direct synchrotron radiation from the radio jet or be scattered nuclear continuum light.

We thank NATO for support under grant 675/83 and the Time Allocation Committee of the University of Hawaii for observing time on the 88 inch telescope. This research was also supported by NASA grant NAG8-529 to the University of Maryland. C. A. H. acknowledges the receipt of an SERC studentship.

REFERENCES

- Adams, T. F., and Weedman, D. W. 1975, *Ap. J.*, **199**, 19.
 Antonucci, R. R. J., and Miller, J. S. 1985, *Ap. J.*, **297**, 621.
 Baldwin, J. A., Wilson, A. S., and Whittle, M. 1987, *Ap. J.*, **319**, 84.
 Balick, B., and Heckman, T. M. 1979, *A.J.*, **84**, 302.
 Binette, L., Dopita, M. A., and Tuohy, I. R. 1985, *Ap. J.*, **297**, 476.
 Carleton, N. P., Elvis, M., Fabbiano, G., Lawrence, A., Ward, M. J., and Willner, S. P. 1987, *Ap. J.*, **318**, 595.
 Cecil, G., Tully, R. B., and Bland, J. 1986, *Bull. AAS.*, **18**, 640.
 Cesar, M. L., Aldrovandi, S. M. V., and Gruenwald, R. 1985, *Pub. A.S.P.*, **97**, 850.
 Code, A. D., Davis, J., Bless, R. C., and Hanbury Brown, R. 1976, *Ap. J.*, **203**, 417.
 Condon, J. J., Condon, M. A., Gisler, G., and Puschell, J. J. 1982, *Ap. J.*, **252**, 102.
 Contini, M., and Aldrovandi, S. M. V. 1983, *Astr. Ap.*, **127**, 15.
 de Bruyn, A. G., and Wilson, A. S. 1976, *Astr. Ap.*, **53**, 93.
 ———. 1978, *Astr. Ap.*, **64**, 433.
 Ferland, G. J. 1981, *Ap. J.*, **249**, 17.
 Ferland, G. J., and Mushotzky, R. F. 1984, *Ap. J.*, **286**, 42.
 Ferland, G. J., and Osterbrock, D. E. 1986, *Ap. J.*, **300**, 658.
 Ferland, G. J., and Shields, G. A. 1985, in *Astrophysics of Active Galaxies and Quasi-Stellar Objects*, ed. J. S. Miller (Mill Valley, CA: University Science Books), p. 157.
 Goodrich, R. W., and Osterbrock, D. E. 1983, *Ap. J.*, **269**, 416.
 Gruenwald, R. B., and Viegas-Aldrovandi, S. M. 1987, *Astr. Ap. Suppl. Ser.*, **70**, 143.
 Haniff, C. A., Wilson, A. S., and Ward, M. J. 1988, *Ap. J.*, **334**, 000 (Paper I).
 Hawley, S. A., and Phillips, M. M. 1980, *Ap. J.*, **235**, 783.
 Koski, A. T. 1978, *Ap. J.*, **223**, 56.
 Kriss, G. A., Canizares, C. R., and Ricker, G. R. 1980, *Ap. J.*, **242**, 492.
 Krolik, J. H., and Begelman, M. C. 1988, *Ap. J.*, **329**, 702.
 MacAlpine, G. M., Williams, G. A., and Lewis, D. W. 1979, *Pub. A.S.P.*, **91**, 746.
 Malkan, M., and Oke, J. B. 1983, *Ap. J.*, **265**, 92.
 Monier, R., and Halpern, J. P. 1987, *Ap. J. (Letters)*, **315**, L17.
 Morris, S. L., Ward, M. J., Whittle, D. M., Wilson, A. S., and Taylor, K. 1985, *M.N.R.A.S.*, **216**, 193.
 Netzer, H. 1987, *M.N.R.A.S.*, **225**, 55.
 Neugebauer, G., et al. 1980, *Ap. J.*, **238**, 502.
 Osterbrock, D. E. 1981, *Ap. J.*, **249**, 462.
 ———. 1983, *IAU Symposium 103, Planetary Nebulae*, ed. D. R. Flower (Dordrecht: Reidel), p. 473.
 Pedlar, A., Dyson, J., and Unger, S. W. 1985, *M.N.R.A.S.*, **214**, 463.
 Penston, M. V., Fosbury, R. A. E., Boksenberg, A., Ward, M. J., and Wilson, A. S. 1984, *M.N.R.A.S.*, **208**, 347.
 Phillips, M. M., Charles, P. A., and Baldwin, J. A. 1983, *Ap. J.*, **266**, 485.
 Phillips, M. M., and Malin, D. F. 1982, *M.N.R.A.S.*, **199**, 905.
 Raymond, J. C. 1979, *Ap. J. Suppl.*, **39**, 1.
 Schommer, R. A., Caldwell, N., Wilson, A. S., Baldwin, J. A., Phillips, M. M., Williams, T. B., and Turtle, A. J. 1987, *Ap. J.*, **324**, 154.
 Scott, J. S., Holman, G. D., Ionson, J. A., and Papadopoulos, K. 1980, *Ap. J.*, **239**, 769.
 Shuder, J. M., and Osterbrock, D. E. 1981, *Ap. J.*, **250**, 55.
 Shull, J. M., and McKee, C. F. 1979, *Ap. J.*, **227**, 131.
 Telesco, C. M., Becklin, E. E., Wynn-Williams, C. G., and Harper, D. A. 1984, *Ap. J.*, **282**, 427.
 Tresch-Fienberg, R., Fazio, G. G., Gezari, D. Y., Hoffmann, W. F., Lamb, G. M., Shu, P. K., and McCreight, C. R. 1987, *Ap. J.*, **312**, 542.
 Ulvestad, J. S. 1981, Ph.D. thesis, University of Maryland.
 ———. 1986, *Ap. J.*, **310**, 136.
 Ulvestad, J. S., Neff, S. G., and Wilson, A. S. 1987, *A.J.*, **93**, 22.
 Ulvestad, J. S., and Wilson, A. S. 1983, *A.J.*, **88**, 253.
 ———. 1984a, *Ap. J.*, **278**, 544.
 ———. 1984b, *Ap. J.*, **285**, 439.
 ———. 1988, *Ap. J. Suppl.*, submitted.
 Unger, S. W., Pedlar, A., Axon, D. J., Whittle, M., Meurs, E. J. A., and Ward, M. J. 1987, *M.N.R.A.S.*, **228**, 671.
 Unger, S. W., Pedlar, A., Booler, R. V., and Harrison, B. A. 1986, *M.N.R.A.S.*, **219**, 387.
 Urry, C. M., Kruper, J. S., Canizares, C. R., Rohan, M. L., and Oberhardt, M. R. 1986, in *Proc. Conf. Variability of Galactic and Extragalactic X-Ray Sources*, ed. A. Treves.
 Walker, M. F. 1968, *Ap. J.*, **151**, 71.
 Whittle, M. 1985, *M.N.R.A.S.*, **213**, 33.
 Whittle, M., Haniff, C. A., Ward, M. J., Meurs, E. J. A., Pedlar, A., Unger, S. W., Axon, D. J., and Harrison, B. A. 1986, *M.N.R.A.S.*, **222**, 189.
 Whittle, M., Pedlar, A., Meurs, E. J. A., Unger, S. W., Axon, D. J., and Ward, M. J. 1988, *Ap. J.*, **326**, 125.
 Wilson, A. S. 1982, *IAU Symposium 97, Extragalactic Radio Sources*, ed. D. S. Heeschen and C. M. Wade (Dordrecht: Reidel), p. 179.
 ———. 1987, *IAU Symposium 121, Observational Evidences of Activity in Galaxies*, ed. E. Ye. Khachikian, K. J. Fricke, and J. Melnick (Dordrecht: Reidel), p. 237.
 Wilson, A. S., Baldwin, J. A., and Ulvestad, J. S. 1985, *Ap. J.*, **291**, 627.
 Wilson, A. S., and Meurs, E. J. A. 1982, *Astr. Ap. Suppl. Ser.*, **50**, 217.
 Wilson, A. S., and Ulvestad, J. S. 1982, *Ap. J.*, **263**, 576.
 ———. 1987, *Ap. J.*, **319**, 105.
 Wu, C.-C., Boggess, A., and Gull, T. R. 1983, *Ap. J.*, **266**, 28.
 Yee, H. K. C. 1980, *Ap. J.*, **241**, 894.

CHRISTOPHER A. HANIFF: Institute of Astronomy, Madingley Road, Cambridge CB3 0HA, England, UK

MARTIN J. WARD: Astronomy Department, FM-20, University of Washington, Seattle, WA 98195

ANDREW S. WILSON: Astronomy Program, University of Maryland, College Park, MD 20742